Middle Rio Grande Physical Modeling

Transverse instream structure analysis: Maximum and average velocity ratios within the prismatic channel

S. Michael Scurlock, Amanda L. Cox, Christopher I. Thornton, and Steven R. Abt

Peer Technical Review by Drew C. Baird, Bureau of Reclamation, Denver Technical Service Center, Denver Colorado

August 2012

Colorado State University
Engineering Research Center
Department of Civil and Environmental Engineering

Middle Rio Grande Physical Modeling

Transverse instream structure analysis: Maximum and average velocity ratios within the prismatic channel

Prepared by:

Colorado State University
Daryl B. Simons Building at the
Engineering Research Center
Fort Collins, Colorado 80523

Prepared for:

U.S. Department of the Interior
Bureau of Reclamation
Albuquerque Area Office
555 Broadway N.E., Suite 100
Albuquerque, New Mexico 87102-2352

This research has been completed at Colorado State University with funding from the U. S. Bureau of Reclamation in Albuquerque, NM, via U. S. Forest Service Contract: 07-JV-221602-264. This research was supported in part by funds provided by the Rocky Mountain Research Station, Forest Service, U. S. Department of Agriculture.

Table of Contents

List of Figures

List of Tables

Executive Summary

Colorado State University constructed a physical model under contract by the United States Bureau of Reclamation in 2001. The purpose of the model was to facilitate evaluation of instream structure hydraulics within channel bends possessing representative plan form characteristics of the Middle Rio Grande River, New Mexico. Spur-dikes, vanes, and submerged spur-dike structures were installed with varying plan-view design characteristics. Time-averaged velocity data were collected within structure configurations and were analyzed to ascertain bend-averaged and maximum values. Processed velocity values were used for the development of ratios identified for the quantification of mean-flow and averaged-flow velocities induced from the instream structures. A ratio of the maximum velocity and a ratio of bend-averaged velocity after structure installation were determined for each structure configuration along the centerline, inner-bank, and outer-bank of the channel bend. A set of influential structure design parameters was identified, organized into dimensionless groupings, and arranged for regression analyses. Suites of predictive equations describing the ratios of maximum velocity and bend-averaged velocity were produced for all structures, spur-dikes, vanes, and submerged spur-dikes. Results of analyses improve upon, and greatly expand previous predictive methodologies. For structure configurations which fall within the ranges of tested data, the prediction equations serve as a first approximation of structure design.

Introduction

River environments are complex and dynamic systems wherein localized and regional geologic, geographic, ecologic, meteoric, and anthropogenic influences dictate the characteristics of the flow path and behavior. In 1975, the Cochiti Dam was installed in a braiding geomorphic regime of the Middle Rio Grande River upstream of Albuquerque, New Mexico. The braiding system present before installation was typical for the distance of the river along its path from its mountainous headwaters, as well as the localized sediment gradation, slope, and vegetation recruitment. The installation of the Cochiti Dam effectively disrupted sediment supply to the downstream reach of the channel, and resulted in a geomorphic shift from a braiding to meandering regime, endangering infrastructure and valuable land holdings. The Albuquerque Area Office of the United States Bureau of Reclamation (Reclamation) identified a variety of instream structures as potential mitigation measures of undesired channel migration within the study reach of the Middle Rio Grande River as depicted in Figure 1**.**

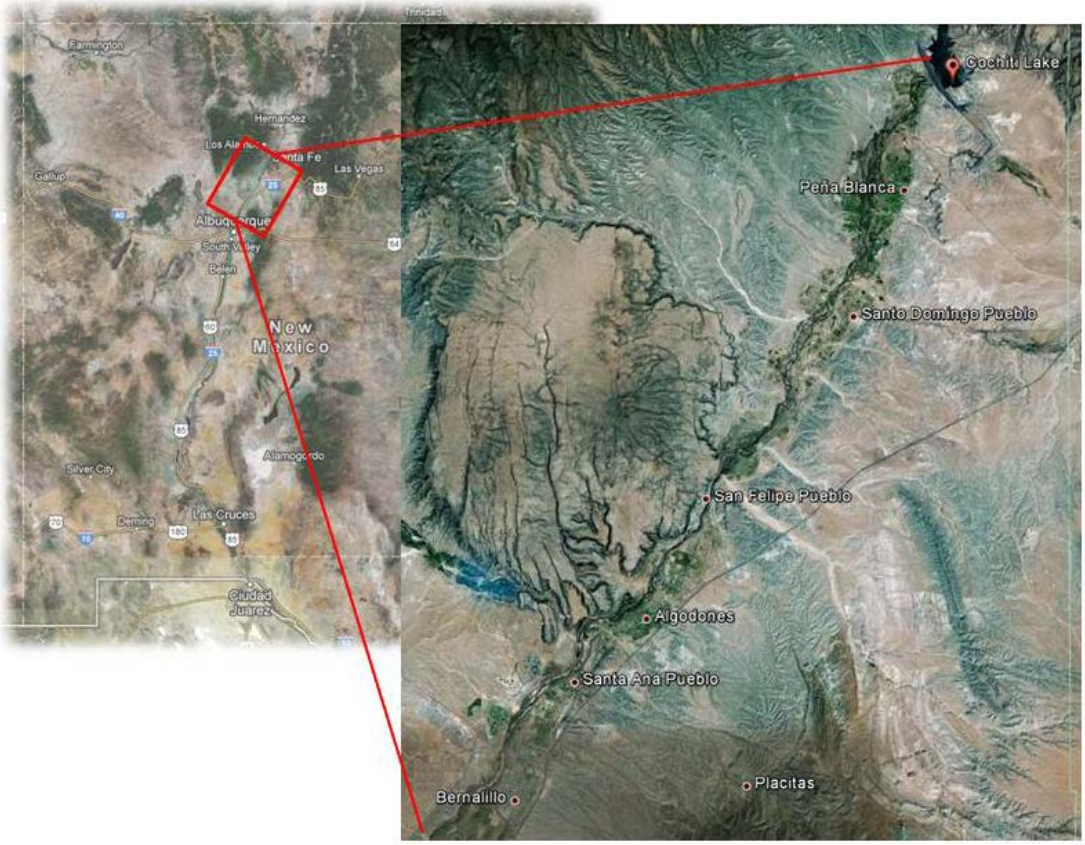

Figure 1. Middle Rio Grande River prototype area (Google, 2012)

Instream structure nomenclature is dependent upon the design elevation of the structure crest relative to the design flow depth, structure plan angle, structure profile angle, and intended purpose. Spur-dikes, vanes, bendway weirs, Iowa vanes, jetties, hardpoints, retards, groynes, guidebanks, and others are structures designed to train channel-bend flows to a desired path (Federal Highway Administration, 2001). Spur-dikes are defined as flat-crested structures,

constructed with the crest set at design flow elevation, which extend from the outer channel bank to the channel center (Lagasse et al., 2001). Bendway weirs are structures which are similar to spur-dikes, yet are designed with the weir crest at approximately one-third to one-half design flow elevation (Lagasse et al., 2001, Julien and Duncan, 2003, McCullah and Gray, 2005). According to Bhuiyan et al. (2010), structures tied into the outer-channel bank of a meandering bend at the design flow elevation, possessing a sloped crest extending into the channel, are designated as vanes.

Instream structures have historically been the focus of analytical, numerical, and physical investigation. Abad et al. (2008) examined various flow stage effects on bendway weirs using numerical modeling validated with field data. Kuhnle et al. (2008) and Jia et al. (2005) performed numerical and physical modeling, and Duan (2009) performed physical modeling, around a single submerged spur dike, identifying flow paths and secondary currents. Bhuiyan et al. (2010) investigated bank-attached vanes and documented resulting scour, turbulence, and velocities from single and multiple structures. Yossef and de Vriend (2011) reported velocity data on a series of spur-dikes in a straight channel. Scott et al. (2001) investigated submerged weir fields with numerical modeling and field data. Ho et al. (2007) numerically investigated the influence of permeability on the hydraulic effects induced by a single groyne. Bhuiyan et al. (2009), Johnson et al. (2001), and Rahman and Haque (2004) document sediment transport effects due to instream structure installations. Han et al. (2011) performed numerical modeling, Odgaard and Splogaric (1986), Odgaard and Mosconi (1987), and Voisin and Townsend (2002) used laboratory data, to describe hydraulic effects of Iowa vanes.

Focusing upon bank-attached, instream structures installed along the outer-bank to reduce flow erosivity, Reclamation contracted Colorado State University (CSU) to conduct a physical model to investigate structure-induced hydraulic conditions. A concrete, trapezoidal, 1:12 Froude-scaled physical model was constructed in 2001 at CSU consisting of two representative channel bends of the Middle Rio Grande placed in series connected with a transition zone. Figure 2 presents a schematic of the planform geometry, and Figure 3 portrays a picture of the constructed prismatic model. Heintz (2002) details the rationale behind the selection of bend geometries and construction methods.

Heintz (2002) installed and collected data on spur-dikes with various geometric configurations. Certain flow rates tested for the constructed spur-dikes reported by Heintz (2002) overtopped the designed crest elevation, producing hydraulic conditions similar to bendway weirs. Spur-dikes with overtopping flow evaluated by Heintz (2002) were set with weir-crest elevations not contained within recommended bendway weir design guidelines. The combination of overtopping flow hydraulics with crest elevations exceeding design guidelines led to the designation of such structures as submerged spur-dikes. Assuming that the structures were appropriate for the flows tested, submerged spur-dikes were set approximately 40% higher than the limiting design criteria of one-half bankfull hydraulic flow depth (Lagasse et al., 2001). Darrow (2004) expanded the work conducted by Heintz to investigate effects of spacing ratios between the structures. Schmidt (2005) reconfigured the spur-dikes and submerged spur-dikes established by Heintz (2002) to include sloping structure crests. Structures evaluated by Schmidt do not exhibit the classic definition of vanes; the tie-in elevation was constructed above any flow elevation evaluated. Traditional vanes, intersecting the bank at the design flow elevation, remain classified as vanes when the flow elevation drops below the design flow elevation. While not tied into the bank at the design discharge, constructed lab structures by Schmidt (2005) still function like vanes at flow elevations lower than those associated with the design discharge, and are

considered as such. Figure 4 provides a plan view of installed structures in a channel bend and Figure 5 shows a cross-section schematic of the spur-dike, submerged spur-dike, and vane structures evaluated in the trapezoidal model.

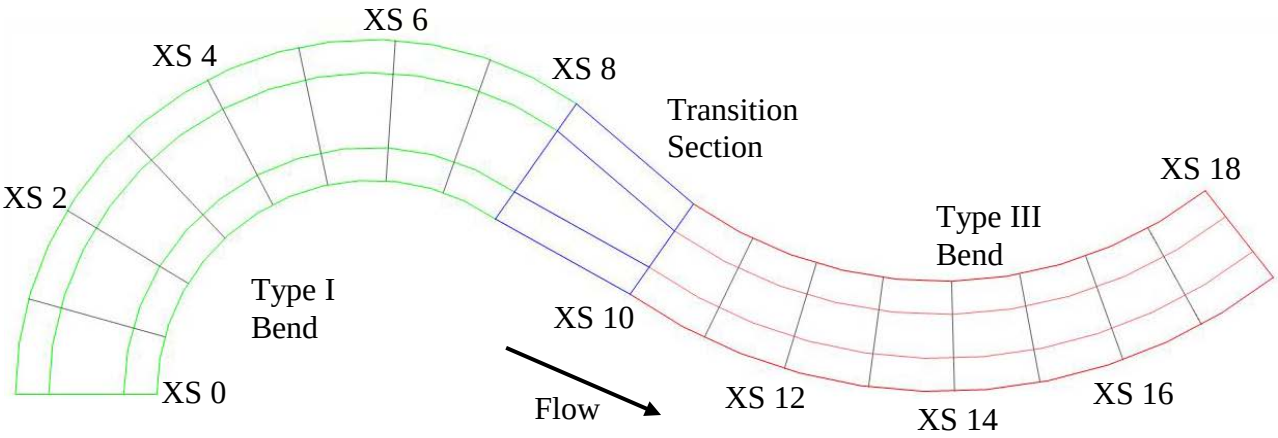

XS = Cross Section

Figure 2. Trapezoidal model plan view

Figure 3. Constructed trapezoidal channel model

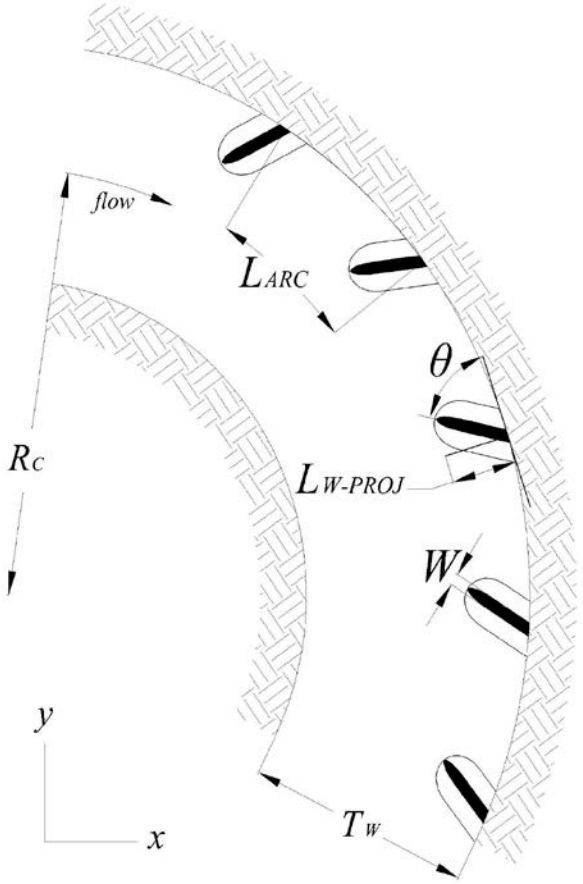

Figure 4. Plan schematic of parameters in Equation 2

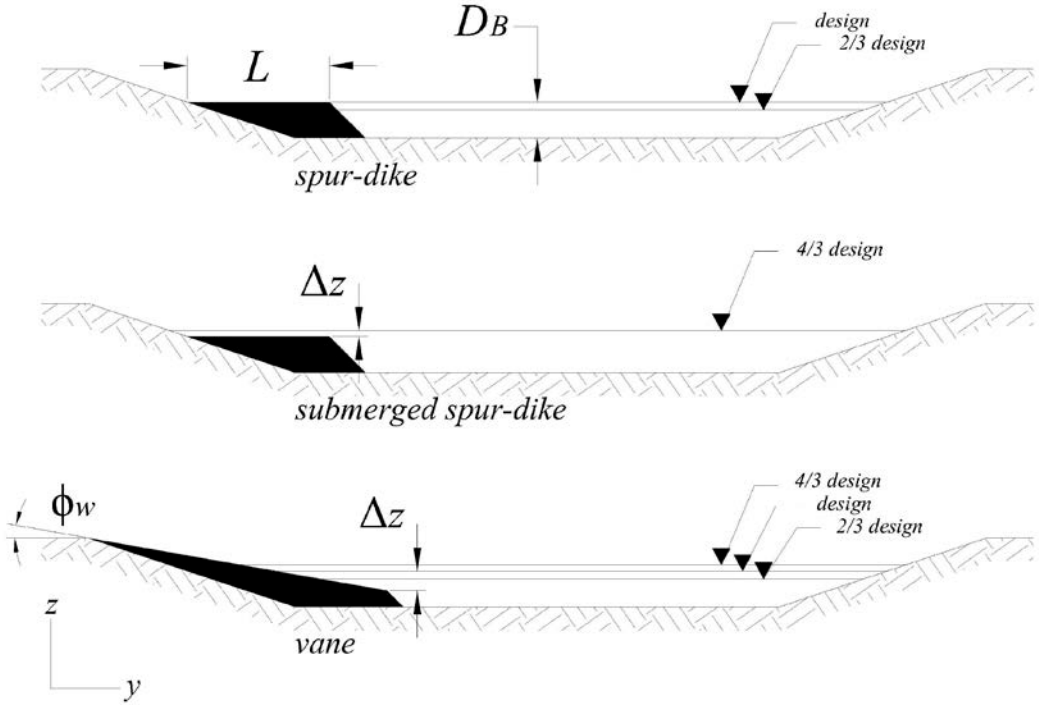

Figure 5. Profile view schematic of evaluated structures in trapezoidal model

Originally defined by Heintz (2002), and then utilized by Darrow (2004) and Schmidt (2005), the concept of the maximum velocity ratio observed within a structure field as compared to baseline conditions was quantified and predictive methodologies were developed. Scurlock et al. (2012) altered the latest iteration of such methodologies and defined the maximum velocity ratio (*MVR*) along the outer-bank of a channel bend with instream structures as:

$$MVR = a_1 + a_2 \ln\left(\frac{L_{ARC}}{T_W}\right) + a_3 \ln\left(\frac{R_C}{T_W}\right) + a_4 \ln\left(\frac{L_{W-PROJ}}{T_W}\right) + a_5 \ln\left(\frac{D_B}{D_B - \Delta z}\right) + a_6 \ln\left(\frac{2\theta}{\pi}\right) \qquad (1)$$

where:

$L_{W\text{-}PROJ}$ = projected length of structure into channel [L];

L_{ARC} = arc length between centerline of structures [L];

R_C = radius of curvature of channel bend centerline [L];

T_W = averaged top width of channel measured at baseline in bend [L];

D_B = averaged maximum cross-section baseline flow depth in bend [L];

Δz = elevation difference between water surface and structure crest at the tip [L];

θ = structure plan angle [radians];and

$a_1,\ldots,a_6$ = regression coefficients.

Moving left to right in Equation 2, dimensionless terms can be elaborated as a structure spacing ratio, a curvature ratio, a contraction ratio, a flow depth to structure height ratio, and a measure of the angle of the structure into the channel. Heintz (2002), Darrow (2004), Schmidt (2005), and Scurlock et al. (2012) researched specific design procedure development for describing maximum outer-bank flow velocities within structure fields; however, provide no information of the hydraulic effects apart from the outer-bank. Performed research reduced the collected velocity data to one point in the structure field, disregarding velocity effects through the bend. Research was further limited by disregarding hydraulic differences of the various structures evaluated, and combining all structure types tested for statistical analyses. The objectives of the current research are to expand the concept of the maximum velocity ratio to account for variability in structure type, channel location, and bend-averaged trends and to develop revised equations for prediction of velocities using laboratory data from the trapezoidal model constructed at CSU.

Transverse instream structure data

The prismatic physical model constructed at CSU housed 130 unique transverse structure installations between the upstream and downstream bend, altering plan form angle, profile angle, discharge, length, and spacing of the structures. Sixty spur-dike, 30 submerged spur-dike, and 40 vane combinations of geometric parameters and flow rates were evaluated. Velocity data were collected around and within instream structure fields using a 25 Hz acoustic Doppler velocimeter (ADV). Data collected in the physical model are detailed in the Appendix.

Figure 6 depicts data collection locations in the upstream bend of the physical model. Data were time-averaged over a minute duration and filtered for erroneous values, resulting in

mean-flow and turbulence values. Mean-flow velocity magnitude data at 60% flow depth measured from the water surface were used for the present analysis. Heintz (2002), Darrow (2004), and Schmidt (2005) detail data collection, instrumentation, and structure configurations in further detail. Figure 7 illustrates interpolated velocity data for an installed spur-dike structure field with three evaluated discharges of 8 ft^3/s, 12 ft^3/s and 16 ft^3/s. The 16 ft^3/s discharge overtopped the structure, resulting in submerged spur-dike hydraulics. Flow velocities increased along the channel with increase in discharge, with zones of highest conveyance at the center and inner-bank regions due to structure installation. Figure 8 depicts velocity for two spur-dike structure configurations evaluated at design flow with the only difference being profile angle. Velocities at the centerline and inner-bank are observed to be higher when structures are aligned normal to the flow direction. Outer-bank velocities appear more erratic, with zones of higher velocity, for the angled structures than for the non-angled counterparts. Figure 9 details the velocity distributions of structures with only crest length altered. The spacing ratio, as a function of the crest length, was maintained constant between the structure configurations. Velocity was higher for larger lengths at the centerline and inner-bank locations, and variability in the distribution of the velocity at the outer-bank was reduced. Velocity magnitudes and distributions were significantly affected by alteration of geometric structure parameters. To provide a tool to quantify the induced velocity distribution from instream structure installation, a mathematical framework describing the maximum and bend-averaged velocities at the inner-bank, centerline, and outer-bank channel was developed.

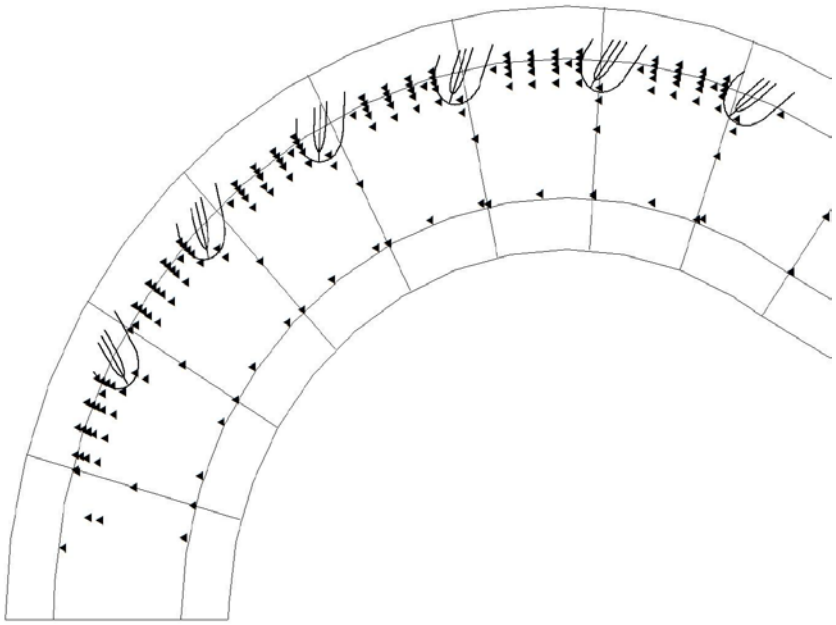

Figure 6. Velocity data collection points around structures in the upstream bend

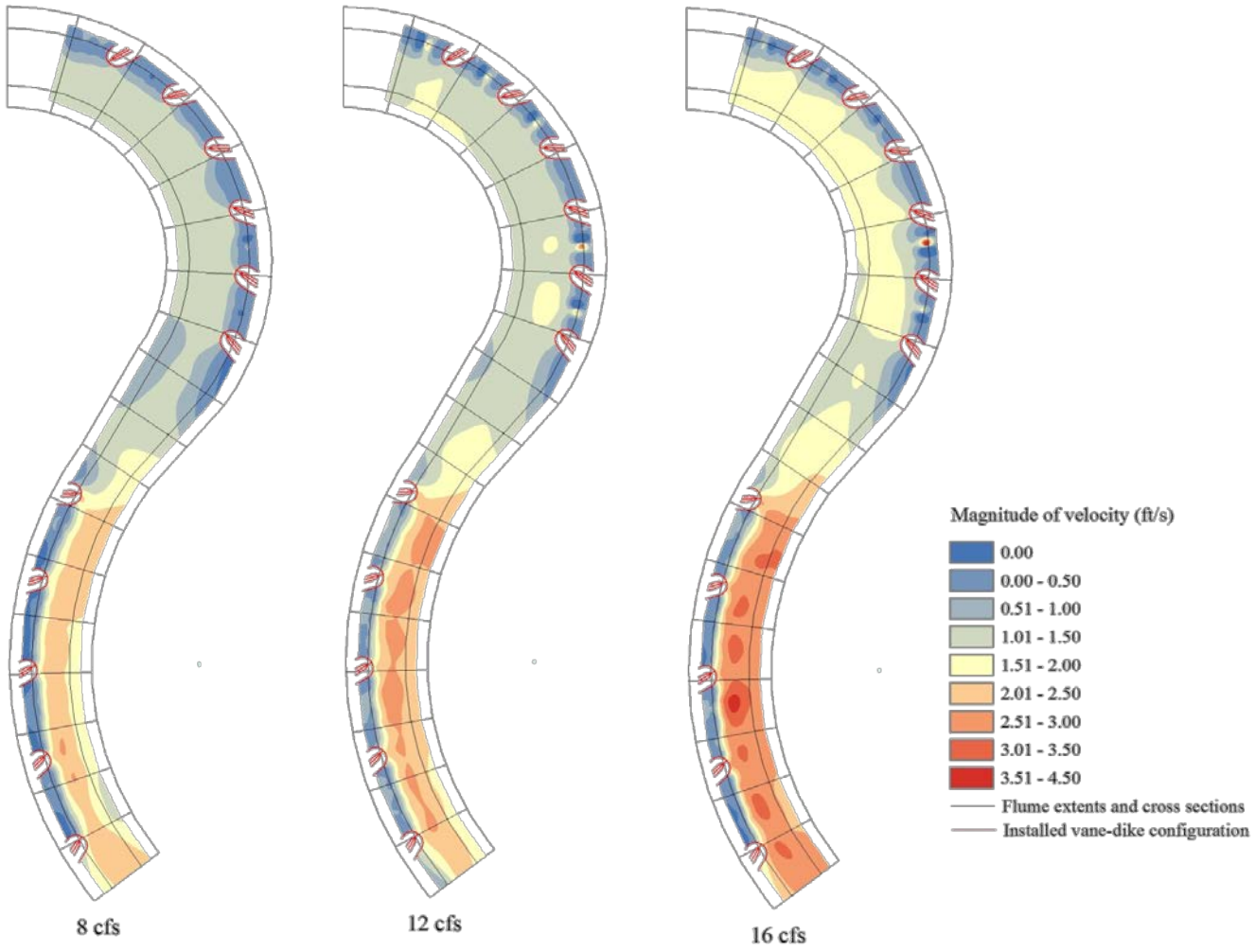

Figure 7. Discharge effects on structure hydraulics

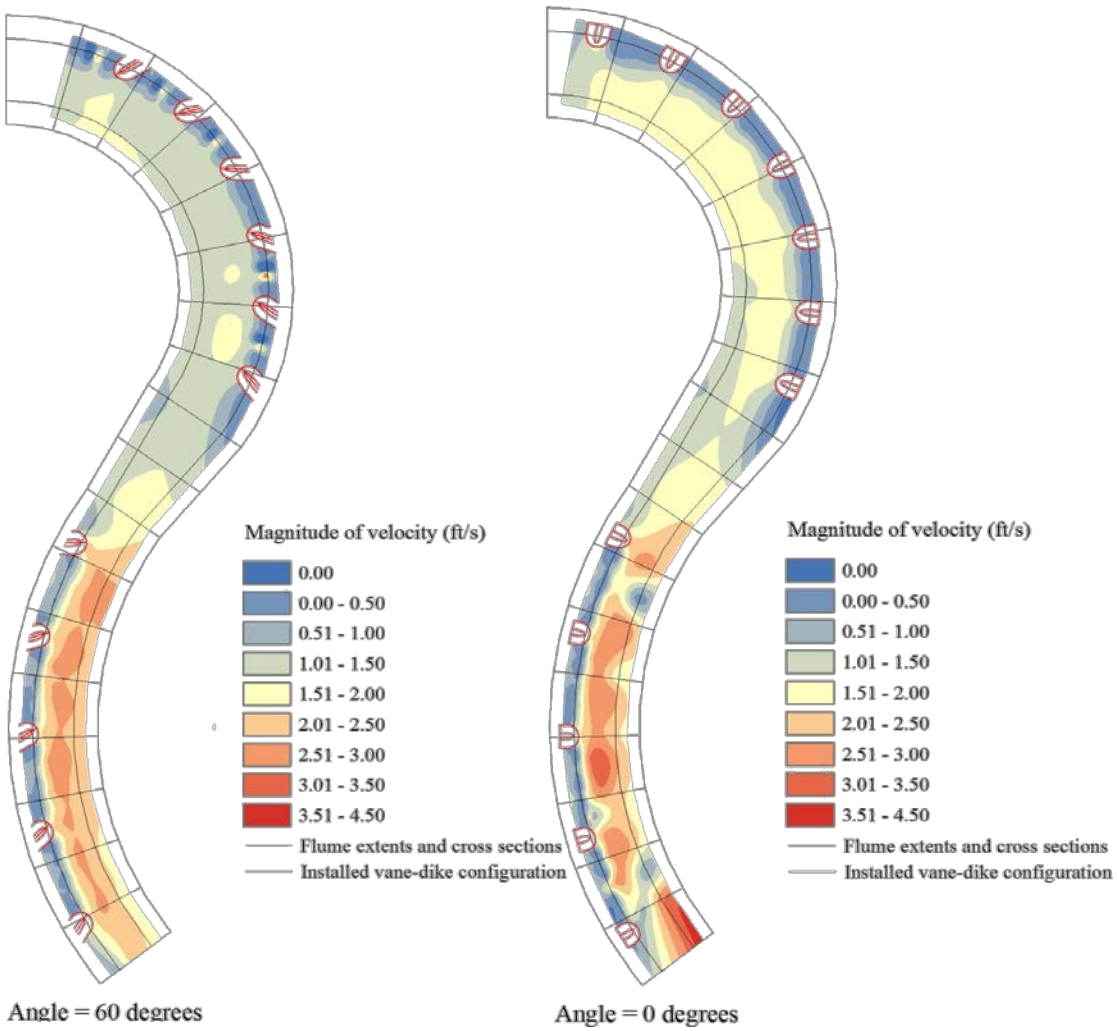

Figure 8. Plan angle effects on structure hydraulics at 12 ft^3/s

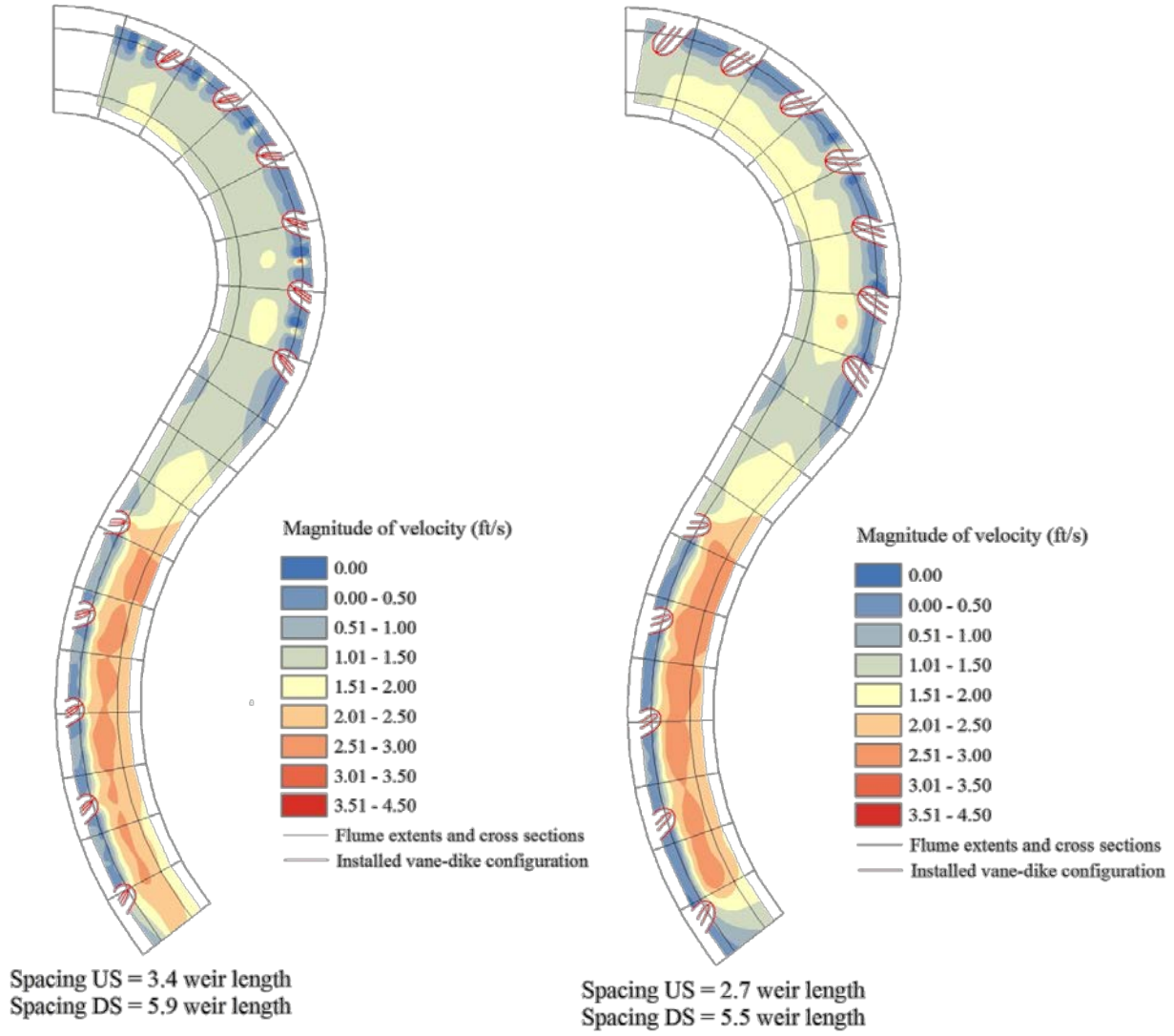

Figure 9. Length effects on structure hydraulics with constant spacing at 12 ft^3/s

Data analysis

Scurlock et al. (2012) established a framework for the prediction of velocity ratios by identifying key geometric parameters of structure design and organizing the parameters into dimensionless groupings with physical meanings. Terms in Equation 1 can be elaborated as a structure spacing ratio, a curvature ratio, a lateral contraction ratio, a vertical contraction ratio, and a normalized structure plan form angle. Dimensionless equation formats have the benefits of invariance due to equation parameter scaling and a lack of dependence on the system of units chosen. Following the concept of *MVR*, the bend-averaged velocity ratio (*AVR*) was defined as Equation 2.

$$AVR = \frac{AV}{V_{Ave\ Baseline}} \tag{2}$$

where:

AV = bend-averaged velocity magnitude [L/T]; and

$V_{Ave\ Basline}$ = baseline cross-sectional averaged velocity along thalweg direction [L/T].

While the concept of *MVR* is important for bank protection and offers an inherent factor of safety for design, bend-averaged velocities may provide a more reliable prediction of the flow hydraulics through the full channel bend by not focusing only on maximum values. Tailoring a mathematical model to data through regression procedures is a process dependent upon how data are scattered relative to the predictive parameters. Non-localized maximum velocitiy data are difficult to capture spatiotemporally, and may behave erratically; therefore, the concept of *AVR* may represent a more reliable predictive method. A benefit of instream structures is navigation improvement through the conveyance shift to the center and inner regions of the channel (Julien, 2002). The use of bend-averaged changes to flow velocities instead of maximum point values are of more importance in such cases.

Scurlock et al. (2012) identified that the upstream channel bend maximum outer-bank velocity data associated with cross-sectional area blockage at design conditions of 27% departed from the trend of the other data to the degree of negatively affecting regression results for the remainder of the full dataset. These data were also excluded from the present analysis of the maximum velocity ratio at the outer-bank. Inclusion of a term in the regression equation model accounting for the percent-area blocked was justified for the remainder of velocity-ratio predictions. The equation format of Scurlock et al. (2012) was altered to a power function for simplicity and overall statistical result benefit, modified to include *AVR*, and augmented with the additional area term as presented in Equation 3.

$$MVR, AVR = a_1 (A^*)^{a_2} \left(\frac{L_{ARC}}{T_W}\right)^{a_3} \left(\frac{R_C}{T_W}\right)^{a_4} \left(\frac{L_{W-PROJ}}{T_W}\right)^{a_5} \left(\frac{D_B}{D_B - \Delta z}\right)^{a_6} \left(\frac{2\theta}{\pi}\right)^{a_7} \tag{3}$$

where:

A^* = percentage of projected cross-sectional weir area to baseline cross-sectional flow area at design flow.

Structures evaluated in the trapezoidal model performed characteristically different due to relative crest elevation to flow depth and crest angle. Spur-dikes, vanes, and submerged spur-dikes were determined to have undergone evaluation, all of which have unique hydraulics and redirect flows away from the outer-bank. Data associated with each structure type was segmented to create unique regression equations. For each structure type, *MVR* and *AVR* were evaluated at the inner-bank, centerline, and outer-bank using backwards linear regression procedures with laboratory data with the methodology of Equation 3. *MVR* and *AVR* prediction equations were also evaluated for all structures combined.

Statistical analysis software was used to perform backwards linear regression on the natural logarithms of collected data at a statistical significance level of $p = 0.05$. The statistical

procedure begins with the full numerical model and then removes the parameter with the least significance, or highest *p*-value above a specified level, determined on the basis of a null *F*-distribution. The model ascribes specific *p*-values to parameters based upon the amount of change generated in the sum of square error, or associated coefficient of determination, when the parameter is either added or removed. Larger *p*-values correspond to smaller changes in the sum of square error when the parameter is added or removed. The truncated numeric model with the largest *p*-value term from the previous model removed will produce a new set of *p*-values for each parameter, and the procedure iterates until all parameters left within the model have associated *p*-values less than the specified level. A *p*-value of 0.05 corresponds to a confidence level of 95% and was used in the regression analysis. Backwards linear regression procedures account for collinearity within the dataset such that two highly correlated terms will not be both included in the final equation form.

Results

Statistical procedures on the form of Equation 3 led to tailored *MVR* and *AVR* equations for each of the structure classes evaluated and a conglomerated equation set. Observed vs. predicted plots of the equations are presented in Figure 10, Figure 11, Figure 12, and Figure 13 for all structure types, spur-dikes, vanes, and submerged spur-dikes, respectively. Table 1 provides *MVR* and *AVR* parameter weights, a_1 through a_7, at the outer-bank, centerline, and inner-bank (subscripts, *o*, *c*, *i*, respectively), the coefficient of determination for the prediction (R^2), and the mean absolute percent error for the prediction (*MA%E*). The number of tests per structure classification utilized during regression procedures is identified in parentheses. Parameter weights of Equation 1 represent the relative importance of a term in the predictive equation; larger values denote parameters with increased significance for that equation. Larger parameter weights do not necessarily denote statistical significance, as incorporation of a parameter into the equation format alters the shape of the multidimensional curve through the parameter space. A value of zero denotes the term being removed from the equation in the statistical process. A value of zero for all equations for a structure classification denotes that the parameter was not altered in the test matrix for that structure. Submerged spur-dikes were not evaluated with flows at various levels over the structure crest; therefore, a_6, the term accounting for this variability was proven statistically insignificant. The relatively low significance of a_2 for the spur-dikes and submerged spur-dikes may indicate a lack of importance of A^* in the definition of induced hydraulics, while for vanes, the term is significant for nearly all predictive equations. It is again noted that the upstream data with cross-sectional area blocked at 27% was removed from MVR_o analyses as detailed by Scurlock et al. (2012). Spur-dike and submerged spur-dike *MVRo* coefficient of determination values increased by 0.229 and 0.200 with the removal of the data, respectively. Fourteen data points were removed from the spur-dike dataset and 7 tests were excluded from the submerged spur-dike dataset. Vanes were not constructed with cross-sectional area blocked exceeding 19.4% and no data were excluded from the structure dataset. Outer-bank velocity ratios were small and showed increasing scatter in prediction towards the lower limits of values, hence high relative error. For specific parameter conditions, there may exist a limit in the estimation of the outer-bank velocity ratios in which predictions cease to provide definitive meaning. In such cases, the outer-bank velocity has been reduced to such an extent that identified predictive parameters do not have distinguishable effects. The prediction of MVR_o resulted in coefficient of determination values of approximately 0.8 for all structure types,

yet the AVR_o prediction performed poorly with the exception of the submerged spur-dikes. Overtopping flow hydraulics associated with submerged spur-dikes were predicted to an overall higher degree of accuracy than the other structure classifications.

Table 1. Regression results

All Data (130)	R^2	*MA%E*	a_1	a_2	a_3	a_4	a_5	a_6	a_7
MVRo	0.8429	20.8533	0.0068	0.0000	0.5546	0.3846	-2.1431	0.7003	0.3824
MVRc	0.8011	4.3100	0.3773	0.2695	0.0000	0.1973	-0.1563	0.0467	0.1155
MVRi	0.6087	4.4433	0.3400	0.3404	-0.1116	0.1065	-0.2084	0.0445	0.1580
AVRo	0.4861	40.7230	0.0138	0.0000	0.5917	0.7439	-1.1451	0.4629	0.5996
AVRc	0.7255	4.0327	0.3615	0.2710	-0.0739	0.1850	-0.1412	0.0536	0.1158
AVRi	0.7530	3.9452	0.1315	0.4894	-0.1308	0.1770	-0.4098	0.1170	0.1266

Spur dike (60)	R^2	*MA%E*	a_1	a_2	a_3	a_4	a_5	a_6	a_7
MVRo	0.8317	20.7074	5.648E-11	3.5354	1.1335	0.0000	-7.8000	-1.9823	0.5963
MVRc	0.9014	3.2235	1.7160	0.0000	-0.0881	0.2674	0.3711	0.1581	0.1970
MVRi	0.6215	4.9464	2.1970	0.0000	-0.0434	0.0000	0.2684	0.2087	0.2253
AVRo	0.7305	28.5942	4.175E-11	3.5645	1.0828	0.0000	-7.5607	-2.1849	0.0000
AVRc	0.7914	3.3918	1.7267	0.0000	-0.1023	0.1758	0.3473	0.1971	0.2053
AVRi	0.7876	3.6910	1.9293	0.0000	-0.1468	0.1512	0.3831	0.4048	0.1835

Vane (40)	R^2	*MA%E*	a_1	a_2	a_3	a_4	a_5	a_6	a_7
MVRo	0.8865	15.7708	9.332E-09	4.1556	0.0000	-0.4323	-5.0082	0.0000	0.5037
MVRc	0.7346	3.1619	0.2301	0.5052	0.0000	0.0000	-2.9864	-0.0592	0.0000
MVRi	0.5455	2.9724	0.3289	0.3993	-0.0603	0.0000	-0.2279	0.0000	0.0000
AVRo	0.3246	50.8338	0.0004	1.3130	-1.9376	2.2401	0.0000	0.0000	1.0996
AVRc	0.6645	3.2535	0.2285	0.4704	0.0000	0.0000	-0.3073	-0.0336	0.0000
AVRi	0.7740	2.4986	0.0313	1.1117	0.0000	-0.2800	-0.7970	-0.1123	0.0000

Submerged spur-dike (30)	R^2	*MA%E*	a_1	a_2	a_3	a_4	a_5	a_6	a_7
MVRo	0.9535	9.2943	5.396E-10	3.0887	0.8140	0.0000	-7.0740	0.0000	0.0000
MVRc	0.9048	3.4581	1.4770	0.0000	0.0000	0.2457	0.2287	0.0000	0.1971
MVRi	0.8103	2.7650	1.8839	0.0000	0.0000	0.0663	0.2059	0.0000	0.2312
AVRo	0.8630	16.1133	0.0073	0.0000	0.7710	0.0000	-2.1743	0.0000	0.0000
AVRc	0.8966	2.4299	0.7546	0.1147	0.0000	0.1529	0.0000	0.0000	0.2002
AVRi	0.8278	3.1874	1.6875	0.0000	0.0000	0.1024	0.2276	0.0000	0.1859

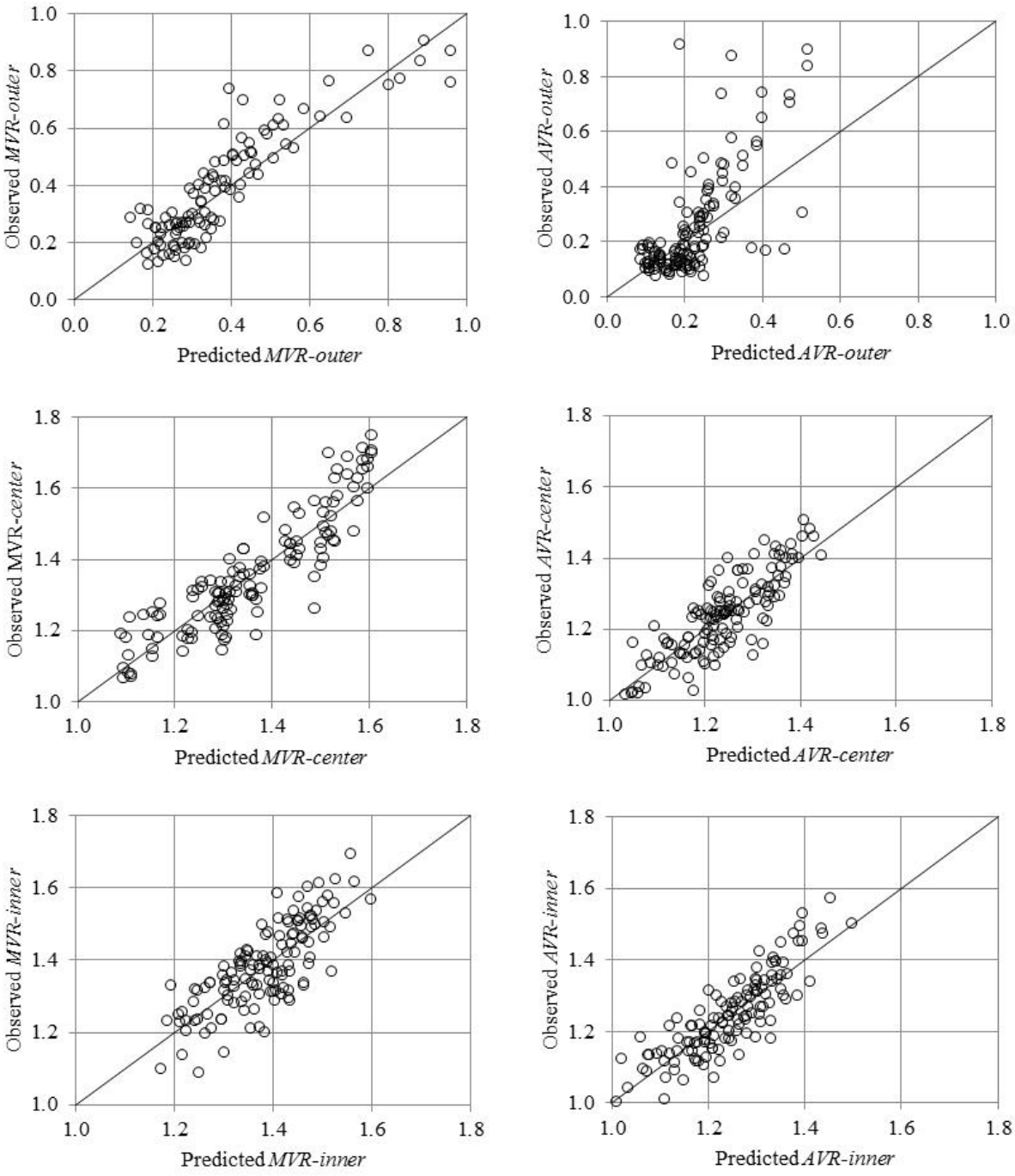

Figure 10. All data regression results: observed vs. predicted *MVR* and *AVR*

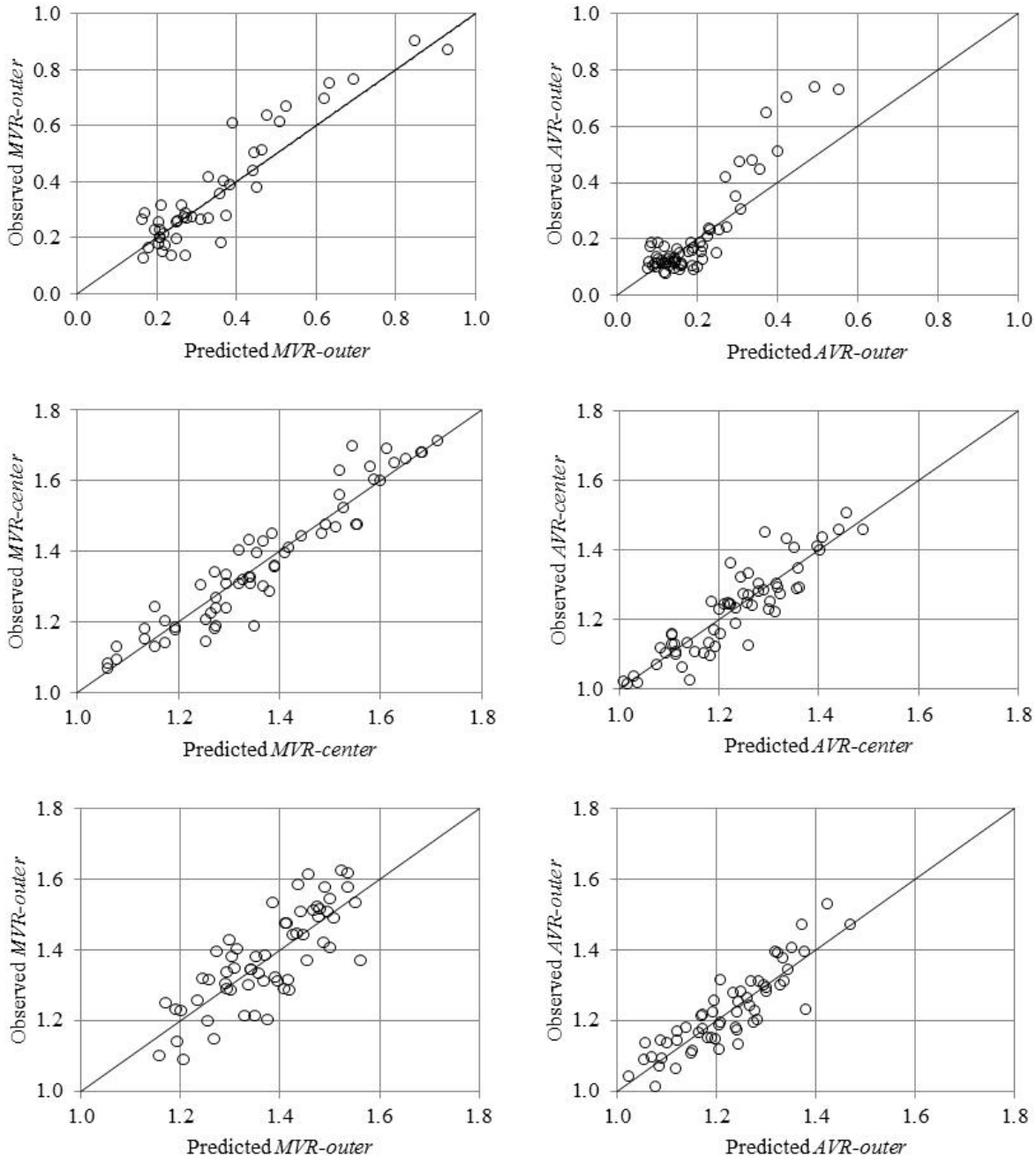

Figure 11. Spur-dike regression results: observed vs. predicted *MVR* and *AVR*

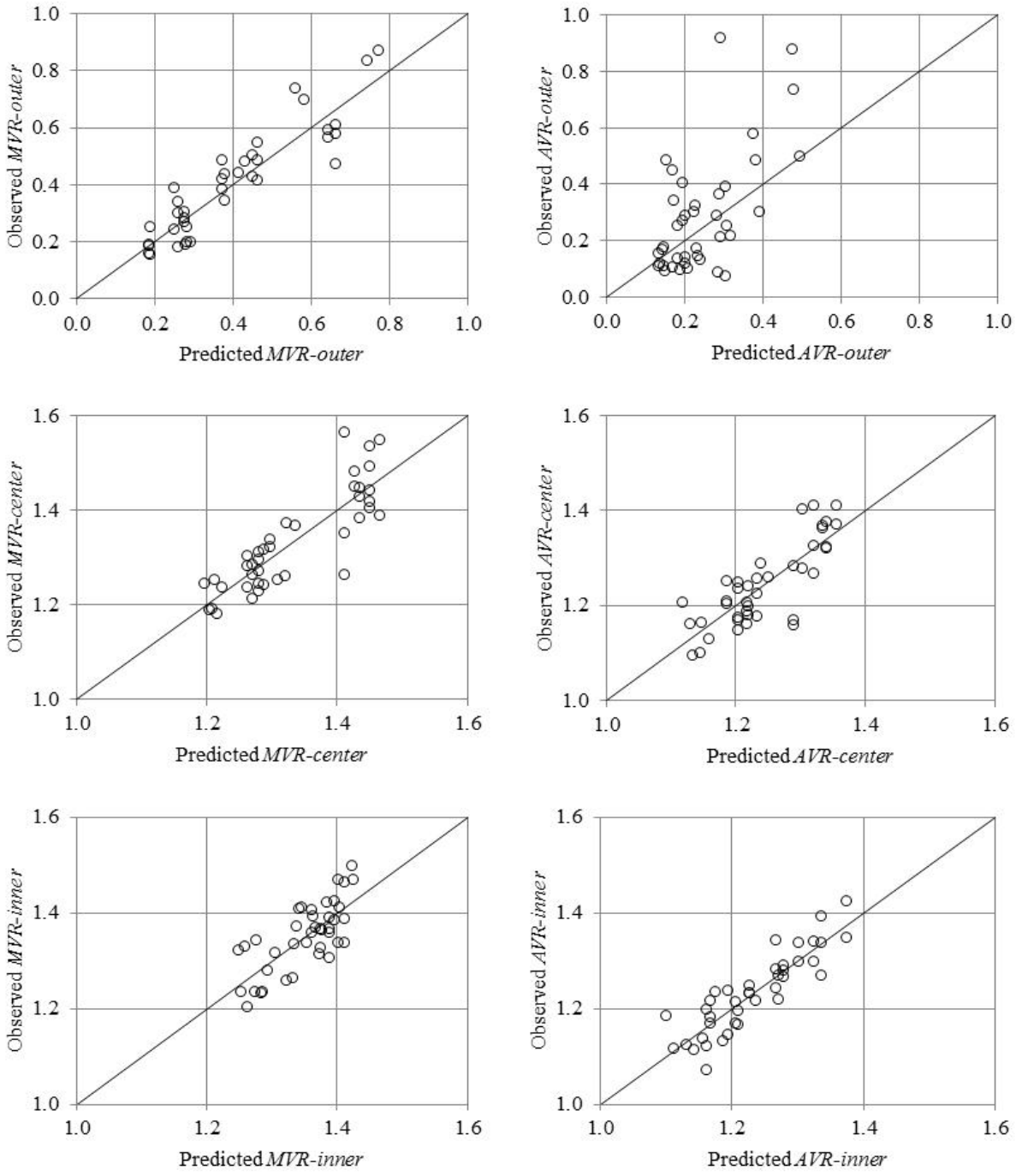

Figure 12. Vane regression results: observed vs. predicted *MVR* and *AVR*

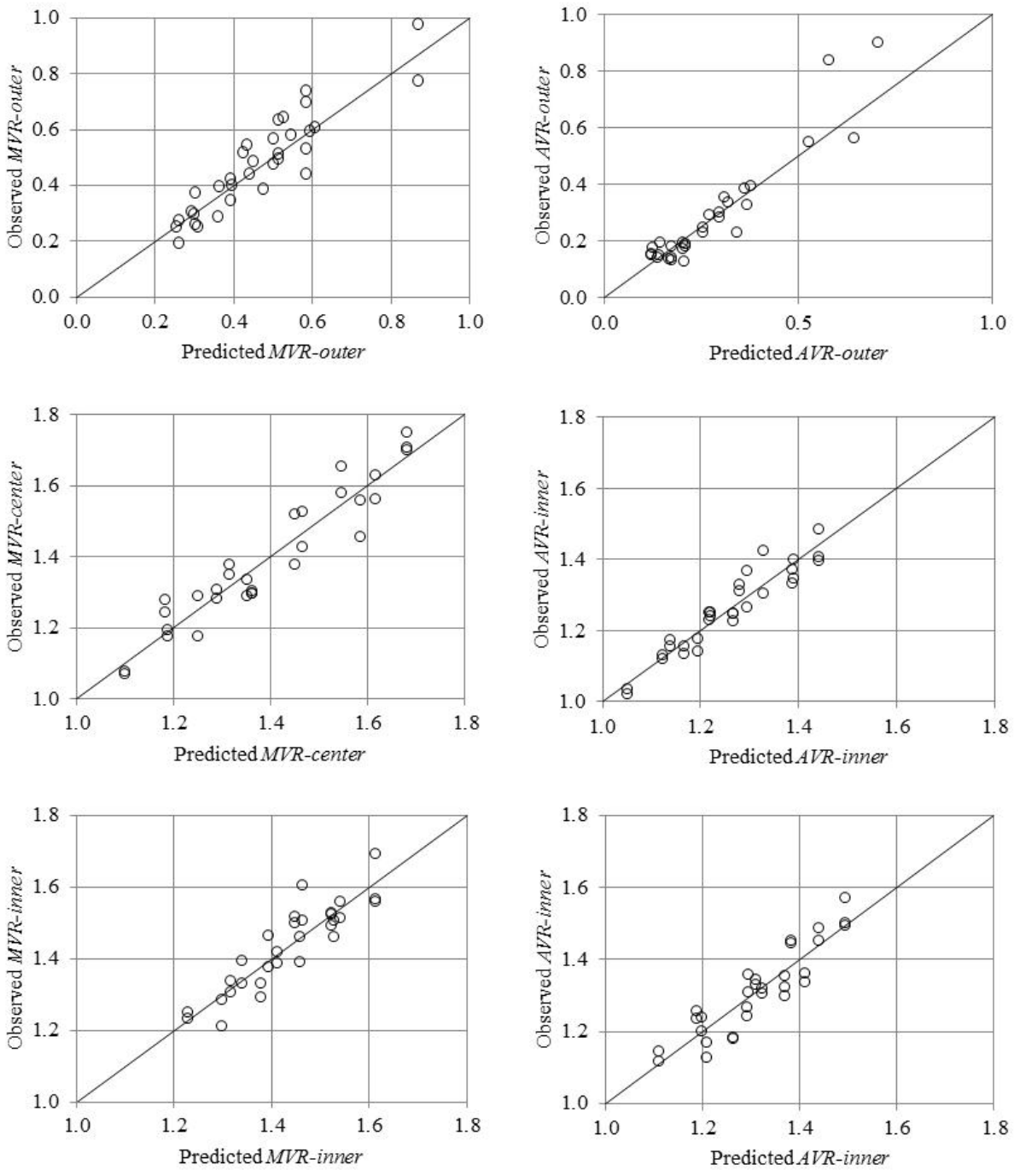

Figure 13. Submerged spur-dike regression results: observed vs. predicted *MVR* and *AVR*

Discussion and recommendations

Spur-dikes, vanes, submerged spur-dikes, and the combined-structure set were analyzed to produce 24 unique design equations for induced structure hydraulics. Scurlock et al. (2012) reported prediction of MVR_o for all structure types with a coefficient of determination of 0.841 and Schmidt (2005) reported prediction of combined-structure MVR_c and MVR_i with coefficients of determination of 0.669 and 0.726, respectively. With regard to coefficient of determination, the proposed model of Equation 3 improves slightly on the previous results for the combined-structure prediction of MVR_o (R^2 = 0.843), improves upon the combined structure MVR_c (R^2 = 0.801), and performs to a lesser degree of accuracy for MVR_i (R^2 = 0.609). Combined-structure AVR_i was predicted with a coefficient of determination value of 0.753.

The equation suites for the vanes and submerged spur-dikes may be laboratory specific due to the structure design not falling within classical definitions. Vane crests extended above the design flow elevation. Structure-specific equations should be used prudently, and if a field or design structure does not resemble laboratory conditions, the generalized equation set likely would better represent hydraulics. To provide a design equation enveloping nearly all of the data to increase safety, offsets based off the error distribution have been determined. Prediction offset by an envelope of two standard deviations of the error distribution accounts for 95.4% of the prediction error assuming a normal distribution. Table 2 provides offset values for the envelope equations calculated for each regression equation, based upon two standard deviations of error. Values should be added to the predicted *MVR* or *AVR* for conservative design.

Table 2. Offset values of two standard deviations of error

All Data	2σ
MVRo	0.2442
MVRc	0.1720
MVRi	0.1665
AVRo	0.4902
AVRc	0.1511
AVRi	0.1424

Spur dike	2σ
MVRo	0.2336
MVRc	0.1424
MVRi	0.1816
AVRo	0.2589
AVRc	0.1413
AVRi	0.1347

Vane	2σ
MVRo	0.1763
MVRc	0.1414
MVRi	0.0918
AVRo	0.5192
AVRc	0.1222
AVRi	0.0903

Submerged spur-dike	2σ
MVRo	0.2911
MVRc	0.1222
MVRi	0.1272
AVRo	0.2362
AVRc	0.0863
AVRi	0.0957

It was observed that certain data behaved erratically, which may further be attributed to associated, large reduction in velocity after structure installation. It was hypothesized that a lower limit of the outer-bank velocity ratios may exist where geometric structure parameters do not have significant impact. From collected data, goodness of fit of the equation visually deteriorates near 0.4 for MVR_o and near 0.2 for AVR_o. The upstream 27% A^* data removed from analysis were comprised of *MVR* values generally below 0.4. Figure 14 graphs a regression equation tailored to the upstream 27% A^* data and the full downstream bend dataset. Determination of the true lower limit of the outer-bank velocity ratios would require further evaluation and data collection, but it is recommended that predicted values of MVR_o and AVR_o below 0.4 and 0.2, respectively, be interpreted cautiously for design purposes.

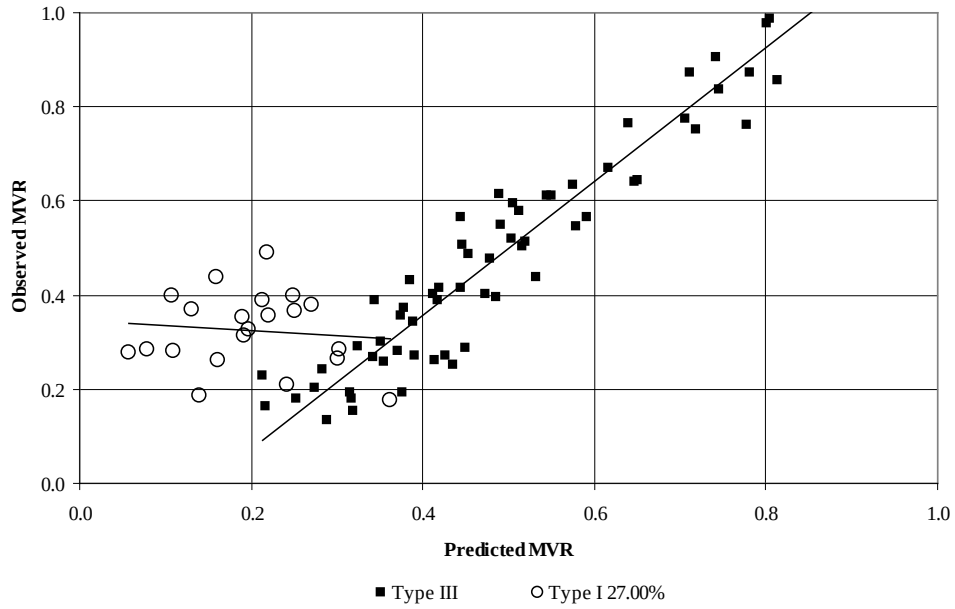

Figure 14. Upstream bend excluded data *MVR*, from Scurlock et al. (2012).

Dimensionless terms used in regression analysis allow for the use of data at any scale and system of units as long as consistency within the equation is maintained. Empirical equations are interpolations based upon the ranges of the data used. In the case of the proposed Equation 3, selected design parameters should fit the dimensionless parameter ranges used for equation development for the methodology to work as intended. Table 3 presents the ranges dimensional parameter values used during laboratory testing and Table 4 gives the terms organized into the

maximum and minimum dimensionless terms utilized for determination of regression coefficients.

Table 3. Dimensional parameter ranges evaluated in laboratory

Structure type	Q (cfs)		L_{ARC} (ft)		T_W (ft)		R_C (ft)		L_{WPROJ} (ft)	
	max	*min*	*max*	*min*	*max*	*min*	*max*	*min*	*max*	*min*
All data	16	8	29.599	8.542	15.630	9.594	65.830	38.750	5.135	1.600
Spur-dike	12	8	29.599	8.542	14.790	9.594	65.830	38.750	4.132	1.600
Vane	16	8	22.060	8.542	15.630	9.594	65.830	38.750	5.135	1.663
Bendway weir	16	16	29.599	8.542	15.630	11.400	65.830	38.750	4.132	1.600

Structure type	Δz (ft)		*Baseline Depth* (ft)		θ (degrees)		*Crest slope* (degrees)	
	max	*min*	*max*	*min*	*max*	*min*	*max*	*min*
All data	0.181	-0.780	0.91	0.60	90	60	10	0
Spur-dike	0.181	0.000	0.78	0.60	90	60	0	0
Vane	-0.093	-0.640	0.78	0.60	90	60	10	10
Bendway weir	-0.120	-0.140	0.91	0.90	90	60	0	0

Table 4. Dimensionless parameter ranges evaluated in laboratory

Structure type	A^*		L_{ARC}/T_W		R_C/T_W		L_{WPROJ}/T_W		D_{RATIO}		$2\theta/\pi$ (rad)	
	max	*min*	*max*	*min*	*max*	*min*	*max*	*min*	*max*	*min*	*max*	*min*
All data	27.00	10.75	3.085	0.547	6.862	2.479	0.373	0.140	6.984	0.768	1.000	0.667
Vane	19.40	10.75	2.299	0.547	6.862	2.479	0.373	0.146	6.984	1.135	1.000	0.667
Spur-dike	27.00	10.75	3.085	0.578	6.862	2.620	0.317	0.150	1.000	0.768	1.000	0.667
Bendway weir	27.00	10.75	2.596	0.547	5.775	2.479	0.267	0.140	1.182	1.154	1.000	0.667

The mathematical model of Equation 3 was shown to be robust in its application to a variety of structure types and flow conditions. Expansion of the regression equations presented in this research through the acquisition of more data would aid in the applicability to a larger set of conditions as well as augment gaps in the current dataset. For instance, only two ratios of R_C/T_W were available due to the constraints of the physical model. As identified through the exclusion of the upstream bend 27% A^* data, but the inclusion of the downstream bend 27% A^* data, values of R_C/T_W are important factors for structure hydraulics. The prismatic nature of the flume lends to efficient creation of numerical models for further evaluation of structures. A validated numerical model using the physical model data would be able to produce any permutation of the parameters of Equation 3 relatively quickly, generating data which would serve as a valuable asset to the research.

Conclusion

Under contract by the United States Bureau, Colorado State University constructed a scaled, prismatic model of two channel bends representative of the Middle Rio Grande River. Spur-dikes, vanes, and submerged spur-dikes were installed in the model and induced hydraulic conditions were quantified and compared to baseline conditions. Two concepts were defined for the description of the velocity effects of the structures: the maximum-velocity ratio, *MVR*, and the bend-averaged velocity ratio, *AVR*. Parameters describing instream structure geometries and channel flows were identified and organized into dimensionless groupings.

Regression procedures were run on a power equation of the dimensionless terms and equations were produced describing *MVR* and *AVR* at the outer-bank, centerline, and inner-bank locations for each structure type independently and combined. Twenty-four unique equations were generated, which generally improve upon existing methodologies when applicable. Envelope equations to increase safety were provided which are based upon the error distribution of the regressions. Equations serve as a first approximation in design and represent the first quantitative structure-specific and bend-averaged tools for structure design. The proposed equation model was verified as applicable to a variety of data and structure-type conditions, and further dataset expansion through field, laboratory, or numerical studies would improve the predictive power of the methodologies.

References

Abad, J.D., Rhoads, B.L., Günerlap, I, and Garcia, M.H. (2008). "Flow structure at different stages in a meander-bend with bendway weirs." *J. Hydraul. Engr.* 134(8). 1052-1063.

Bhuiyan, F., Hey, R.D., and Wormleaton, P.R. (2009). "Effects of vanes and w-weir on sediment transport in meandering channels." *J. Hydraul. Engr.* 135(5). 339-349.

Bhuiyan, F., Hey, R.D., and Wormleaton, P.R. (2010). "Bank-attached vanes for bank erosion control and restoration of river meanders." *J. Hydraul. Engr.* 136(9). 583-596.

Darrow, J.D. (2004). "Effects of bendway weir characteristics on resulting flow conditions." M. S. Thesis. Colorado State University, Department of Civil Engineering. Fort Collins, Colorado.

Duan, J. (2009). "Mean flow and turbulence around a laboratory spur dike." *J. Hydraul. Engr.* 135(10). 803-811.

Federal Highway Administration (2001). "River engineering for highway encroachments: Highways in the river environment." *Hydraulic Design Series Number 6.* U.S. Department of Transportation.

Han, S.S., Ramamurthy, A.S., and Biron, P.M. (2011). "Characteristics of flow around open channel 90º bends with vanes." *J. Hydraul. Engr.* 137(10). 668-676.

Heintz, M.L. (2002). "Investigation of bendway weir spacing." M. S. Thesis. Colorado State University, Department of Civil Engineering. Fort Collins, Colorado.

Ho, J., Yeo, H.K., Coonrod, J., and Ahn, W. (2007). *Proc. Congress-international Assoc. Hydraul. Res.* 32(2).

Jia, Y., Scott, S., Xu, Y. Huang, S., and Wang, S.S.Y. (2005). "Three-dimensional numerical simulation and analysis of flows around a submerged weir in a channel bendway." *J. Hydraul. Engr.* 131(8). 682-693.

Johnson, P.A., Hey, R.D., Tessier, M., and Rosgen, D.L. (2001). "Use of vanes for control of scour at vertical wall abutments." *J. Hydraul. Engr.* 127(9). 772-778.

Julien, P.Y. (2002). River Mechanics. Cambridge University Press. New York, NY.

Julien, P.Y. and Duncan, J.R. (2003). "Optimal design criteria of bendway weirs from numerical simulations and physical model studies." Colorado State University, Department of Civil Engineering. Fort Collins, Colorado.

Kuhnle, R.A., Jia, Y., and Alonso, C.V. (2008). "Measured and simulated flow near a submerged spur dike." *J. Hydraul. Engr.* 134(7). 916-924.

Lagasse, P.F., Clopper, P.E., Zevenbergen, L.W., and Schall, J.D., 2009. "Bridge Scour and Stream Instability Countermeasures," Volume 1 (Third Edition), Publication FHWA-NHI, Federal Highway Administration.

McCullah, J.A. and Gray, D. (2005), "Environmentally Sensitive Channel- and Bank-Protection Measures," NCHRP Report 544, Transportation Research Board, National Academies of Science, Washington, D.C.

Odgaard, J.A., and Mosconi, C.E. (1986). "Streambank protection by submerged vanes." *J. Hydraul. Engr.* 113(4). 520-536.

Odgaard, J.A., and Spoljaric, A. (1986). "Sediment control by submerged vanes." *J. Hydraul. Engr.* 112(12). 1164-1181.

Rahman, M.M., and Haque, M.A. (2004). "Local scour at sloped-wall spur-dike-like structures in alluvial rivers." *J. Hydraul. Engr.* 130(1). 70-74.

Schmidt, P.G. (2005). "Effects of bendway weir field geometry characteristics on channel flow conditions." M. S. Thesis. Colorado State University, Department of Civil Engineering. Fort Collins, Colorado.

Scott, S.H., Jia, Y., Wang, S.S.Y., and Xu, Y. (2001). "Analysis of near-field hydrodynamics of submerged weirs." US Army Corps of Engineers. ERDC/CHL CHETN-VII-1.

Scurlock, S.M., Cox, A.L., Baird, D.C., and Thornton, C.I. (2012). "Middle Rio Grande physical modeling – Transverse instream structure analysis: Maximum outer-bank velocity reduction within the prismatic channel." Colorado State University, Department of Civil Engineering. Fort Collins, CO.

Source: "Middle Rio Grande River." 35°26'39.79" N and 106°27'50.93" W. Google Earth. May 4th, 2012. July 25th, 2012.

Voisin, A., and Townsend, R.D. (2002). "Model testing of submerged vanes in strongly curved narrow channel bends." *Can. J. Civ. Eng.* 29. 37-49.

Walker, K.G. (2009). "Comparison of a generalized trapezoidal model to a native topography patterned bed surface model of the Rio Grande." M. S. technical report. Colorado State University, Department of Civil Engineering. Fort Collins, CO.

Yossef, M.F.M., de Vriend, H.J. (2011). "Flow details near river groynes: experimental investigation." *J. Hydraul. Engr.* 137(5). 504-516.

Appendix

Table 5A. Configuration discharge and geometric parameters

Test no	*Test ID*	*Bend*	*Q*	ö$_W$	è	R_C	L_{ARC}	L_{WPROJ}	T_W	D_B	*Äz*	*A**
-	-	-	*ft³/s*	*rad*	*rad*	*ft*	*ft*	*ft*	*ft*	*ft*	*ft*	-
1	W03	Type I	8	0.000	1.571	38.75	14.03	4.13	13.764	0.599	0.171	27
2	W03	Type I	12	0.000	1.571	38.75	14.03	4.13	14.79	0.77	0.000	27
3	W03	Type I	16	0.000	1.571	38.75	14.03	4.13	15.63	0.91	-0.140	27
4	W03	Type III	8	0.000	1.571	65.83	16.74	3.04	9.594	0.599	0.181	27
5	W03	Type III	12	0.000	1.571	65.83	16.74	3.04	10.68	0.78	0.000	27
6	W03	Type III	16	0.000	1.571	65.83	16.74	3.04	11.4	0.9	-0.120	27
7	W02	Type I	8	0.000	1.571	38.75	21.08	4.13	13.764	0.599	0.171	27
8	W02	Type I	12	0.000	1.571	38.75	21.08	4.13	14.79	0.77	0.000	27
9	W02	Type I	16	0.000	1.571	38.75	21.08	4.13	15.63	0.91	-0.140	27
10	W02	Type III	8	0.000	1.571	65.83	29.60	3.04	9.594	0.599	0.181	27
11	W02	Type III	12	0.000	1.571	65.83	29.60	3.04	10.68	0.78	0.000	27
12	W02	Type III	16	0.000	1.571	65.83	29.60	3.04	11.4	0.9	-0.120	27
13	W01	Type I	8	0.000	1.571	38.75	16.88	4.13	13.764	0.599	0.171	27
14	W01	Type I	12	0.000	1.571	38.75	16.88	4.13	14.79	0.77	0.000	27
15	W01	Type I	16	0.000	1.571	38.75	16.88	4.13	15.63	0.91	-0.140	27
16	W01	Type III	8	0.000	1.571	65.83	20.90	3.04	9.594	0.599	0.181	27
17	W01	Type III	12	0.000	1.571	65.83	20.90	3.04	10.68	0.78	0.000	27
18	W01	Type III	16	0.000	1.571	65.83	20.90	3.04	11.4	0.9	-0.120	27
19	W04	Type I	8	0.000	1.571	38.75	8.54	2.22	13.764	0.599	0.171	10.75
20	W04	Type I	12	0.000	1.571	38.75	8.54	2.22	14.79	0.77	0.000	10.75
21	W04	Type I	16	0.000	1.571	38.75	8.54	2.22	15.63	0.91	-0.140	10.75
22	W04	Type III	8	0.000	1.571	65.83	12.99	1.6	9.594	0.599	0.181	10.75
23	W04	Type III	12	0.000	1.571	65.83	12.99	1.6	10.68	0.78	0.000	10.75
24	W04	Type III	16	0.000	1.571	65.83	12.99	1.6	11.4	0.9	-0.120	10.75
25	W05	Type I	8	0.000	1.571	38.75	10.30	2.22	13.764	0.599	0.171	10.75
26	W05	Type I	12	0.000	1.571	38.75	10.30	2.22	14.79	0.77	0.000	10.75
27	W05	Type I	16	0.000	1.571	38.75	10.30	2.22	15.63	0.91	-0.140	10.75
28	W05	Type III	8	0.000	1.571	65.83	16.78	1.6	9.594	0.599	0.181	10.75
29	W05	Type III	12	0.000	1.571	65.83	16.78	1.6	10.68	0.78	0.000	10.75
30	W05	Type III	16	0.000	1.571	65.83	16.78	1.6	11.4	0.9	-0.120	10.75
31	W06	Type I	8	0.000	1.571	38.75	11.49	3.25	13.764	0.599	0.171	19.4
32	W06	Type I	12	0.000	1.571	38.75	11.49	3.25	14.79	0.77	0.000	19.4
33	W06	Type I	16	0.000	1.571	38.75	11.49	3.25	15.63	0.91	-0.140	19.4
34	W06	Type III	8	0.000	1.571	65.83	17.07	2.35	9.594	0.599	0.181	19.4
35	W06	Type III	12	0.000	1.571	65.83	17.07	2.35	10.68	0.78	0.000	19.4
36	W06	Type III	16	0.000	1.571	65.83	17.07	2.35	11.4	0.9	-0.120	19.4
37	W07	Type I	8	0.000	1.571	38.75	13.85	3.25	13.764	0.599	0.171	19.4
38	W07	Type I	12	0.000	1.571	38.75	13.85	3.25	14.79	0.77	0.000	19.4
39	W07	Type I	16	0.000	1.571	38.75	13.85	3.25	15.63	0.91	-0.140	19.4

Test no	*Test ID*	*Bend*	*Q*	ö$_W$	è	R_C	L_{ARC}	L_{WPROJ}	T_W	D_B	*Äz*	*A**
-	-	-	*ft³/s*	*rad*	*rad*	*ft*	*ft*	*ft*	*ft*	*ft*	*ft*	-
40	W07	Type III	8	0.000	1.571	65.83	22.06	2.35	9.594	0.599	0.181	19.4
41	W07	Type III	12	0.000	1.571	65.83	22.06	2.35	10.68	0.78	0.000	19.4
42	W07	Type III	16	0.000	1.571	65.83	22.06	2.35	11.4	0.9	-0.120	19.4
43	W08	Type I	8	0.000	1.047	38.75	8.54	2.295	13.764	0.599	0.171	10.75
44	W08	Type I	12	0.000	1.047	38.75	8.54	2.295	14.79	0.77	0.000	10.75
45	W08	Type I	16	0.000	1.047	38.75	8.54	2.295	15.63	0.91	-0.140	10.75
46	W08	Type III	8	0.000	1.047	65.83	12.99	1.67	9.594	0.599	0.181	10.75
47	W08	Type III	12	0.000	1.047	65.83	12.99	1.67	10.68	0.78	0.000	10.75
48	W08	Type III	16	0.000	1.047	65.83	12.99	1.67	11.4	0.9	-0.120	10.75
49	W09	Type I	8	0.000	1.047	38.75	10.30	2.295	13.764	0.599	0.171	10.75
50	W09	Type I	12	0.000	1.047	38.75	10.30	2.295	14.79	0.77	0.000	10.75
51	W09	Type I	16	0.000	1.047	38.75	10.30	2.295	15.63	0.91	-0.140	10.75
52	W09	Type III	8	0.000	1.047	65.83	16.78	1.67	9.594	0.599	0.181	10.75
53	W09	Type III	12	0.000	1.047	65.83	16.78	1.67	10.68	0.78	0.000	10.75
54	W09	Type III	16	0.000	1.047	65.83	16.78	1.67	11.4	0.9	-0.120	10.75
55	W10	Type I	8	0.000	1.047	38.75	11.18	3.227	13.764	0.599	0.171	19.4
56	W10	Type I	12	0.000	1.047	38.75	11.18	3.227	14.79	0.77	0.000	19.4
57	W10	Type I	16	0.000	1.047	38.75	11.18	3.227	15.63	0.91	-0.140	19.4
58	W10	Type III	8	0.000	1.047	65.83	16.49	2.365	9.594	0.599	0.181	19.4
59	W10	Type III	12	0.000	1.047	65.83	16.49	2.365	10.68	0.78	0.000	19.4
60	W10	Type III	16	0.000	1.047	65.83	16.49	2.365	11.4	0.9	-0.120	19.4
61	W11	Type I	8	0.000	1.047	38.75	13.48	3.227	13.764	0.599	0.171	19.4
62	W11	Type I	12	0.000	1.047	38.75	13.48	3.227	14.79	0.77	0.000	19.4
63	W11	Type I	16	0.000	1.047	38.75	13.48	3.227	15.63	0.91	-0.140	19.4
64	W11	Type III	8	0.000	1.047	65.83	21.30	2.365	9.594	0.599	0.181	19.4
65	W11	Type III	12	0.000	1.047	65.83	21.30	2.365	10.68	0.78	0.000	19.4
66	W11	Type III	16	0.000	1.047	65.83	21.30	2.365	11.4	0.9	-0.120	19.4
67	W12	Type I	8	0.000	1.047	38.75	13.70	4.037	13.764	0.599	0.171	27
68	W12	Type I	12	0.000	1.047	38.75	13.70	4.037	14.79	0.77	0.000	27
69	W12	Type I	16	0.000	1.047	38.75	13.70	4.037	15.63	0.91	-0.140	27
70	W12	Type III	8	0.000	1.047	65.83	20.28	2.992	9.594	0.599	0.181	27
71	W12	Type III	12	0.000	1.047	65.83	20.28	2.992	10.68	0.78	0.000	27
72	W12	Type III	16	0.000	1.047	65.83	20.28	2.992	11.4	0.9	-0.120	27
73	W13	Type I	8	0.000	1.047	38.75	16.52	4.037	13.764	0.599	0.171	27
74	W13	Type I	12	0.000	1.047	38.75	16.52	4.037	14.79	0.77	0.000	27
75	W13	Type I	16	0.000	1.047	38.75	16.52	4.037	15.63	0.91	-0.140	27
76	W13	Type III	8	0.000	1.047	65.83	26.19	2.992	9.594	0.599	0.181	27
77	W13	Type III	12	0.000	1.047	65.83	26.19	2.992	10.68	0.78	0.000	27
78	W13	Type III	16	0.000	1.047	65.83	26.19	2.992	11.4	0.9	-0.120	27
79	W14	Type I	8	0.000	1.309	38.75	13.95	4.132	13.764	0.599	0.171	27
80	W14	Type I	12	0.000	1.309	38.75	13.95	4.132	14.79	0.77	0.000	27
81	W14	Type I	16	0.000	1.309	38.75	13.95	4.132	15.63	0.91	-0.140	27
82	W14	Type III	8	0.000	1.309	65.83	20.43	2.993	9.594	0.599	0.181	27
83	W14	Type III	12	0.000	1.309	65.83	20.43	2.993	10.68	0.78	0.000	27
84	W14	Type III	16	0.000	1.309	65.83	20.43	2.993	11.4	0.9	-0.120	27
85	W15	Type I	8	0.000	1.309	38.75	16.82	4.132	13.764	0.599	0.171	27
86	W15	Type I	12	0.000	1.309	38.75	16.82	4.132	14.79	0.77	0.000	27

Test no	*Test ID*	*Bend*	*Q*	ö$_W$	è	R_C	L_{ARC}	L_{WPROJ}	T_W	D_B	*Äz*	*A**
-	-	-	*ft³/s*	*rad*	*rad*	*ft*	*ft*	*ft*	*ft*	*ft*	*ft*	-
87	W15	Type I	16	0.000	1.309	38.75	16.82	4.132	15.63	0.91	-0.140	27
88	W15	Type III	8	0.000	1.309	65.83	26.39	2.993	9.594	0.599	0.181	27
89	W15	Type III	12	0.000	1.309	65.83	26.39	2.993	10.68	0.78	0.000	27
90	W15	Type III	16	0.000	1.309	65.83	26.39	2.993	11.4	0.9	-0.120	27
91	W17	Type I	8	0.175	1.571	38.75	11.49	5.135	13.764	0.599	-0.469	19.4
92	W17	Type I	12	0.175	1.571	38.75	11.49	5.135	14.79	0.77	-0.640	19.4
93	W17	Type I	16	0.175	1.571	38.75	11.49	5.135	15.63	0.91	-0.780	19.4
94	W17	Type III	8	0.175	1.571	65.83	17.07	3.106	9.594	0.599	-0.181	19.4
95	W17	Type III	12	0.175	1.571	65.83	17.07	3.106	10.68	0.78	-0.362	19.4
96	W17	Type III	16	0.175	1.571	65.83	17.07	3.106	11.4	0.9	-0.482	19.4
97	W18	Type I	8	0.175	1.047	38.75	11.49	4.914	13.764	0.599	-0.469	19.4
98	W18	Type I	12	0.175	1.047	38.75	11.49	4.914	14.79	0.77	-0.640	19.4
99	W18	Type I	16	0.175	1.047	38.75	11.49	4.914	15.63	0.91	-0.780	19.4
100	W18	Type III	8	0.175	1.047	65.83	17.07	2.999	9.594	0.599	-0.181	19.4
101	W18	Type III	12	0.175	1.047	65.83	17.07	2.999	10.68	0.78	-0.362	19.4
102	W18	Type III	16	0.175	1.047	65.83	17.07	2.999	11.4	0.9	-0.482	19.4
103	W19	Type I	8	0.175	1.571	38.75	13.85	5.135	13.764	0.599	-0.469	19.4
104	W19	Type I	12	0.175	1.571	38.75	13.85	5.135	14.79	0.77	-0.640	19.4
105	W19	Type I	16	0.175	1.571	38.75	13.85	5.135	15.63	0.91	-0.780	19.4
106	W19	Type III	8	0.175	1.571	65.83	22.06	3.106	9.594	0.599	-0.181	19.4
107	W19	Type III	12	0.175	1.571	65.83	22.06	3.106	10.68	0.78	-0.362	19.4
108	W19	Type III	16	0.175	1.571	65.83	22.06	3.106	11.4	0.9	-0.482	19.4
109	W20	Type I	8	0.175	1.047	38.75	13.48	4.914	13.764	0.599	-0.469	19.4
110	W20	Type I	12	0.175	1.047	38.75	13.48	4.914	14.79	0.77	-0.640	19.4
111	W20	Type I	16	0.175	1.047	38.75	13.48	4.914	15.63	0.91	-0.780	19.4
112	W20	Type III	8	0.175	1.047	65.83	21.30	2.999	9.594	0.599	-0.181	19.4
113	W20	Type III	12	0.175	1.047	65.83	21.30	2.999	10.68	0.78	-0.362	19.4
114	W20	Type III	16	0.175	1.047	65.83	21.30	2.999	11.4	0.9	-0.482	19.4
115	W21	Type I	8	0.175	1.571	38.75	8.54	2.88	13.764	0.599	-0.161	10.75
116	W21	Type I	12	0.175	1.571	38.75	8.54	2.88	14.79	0.77	-0.332	10.75
117	W21	Type I	16	0.175	1.571	38.75	8.54	2.88	15.63	0.91	-0.472	10.75
118	W21	Type III	12	0.175	1.571	65.83	16.78	1.719	10.68	0.78	-0.093	10.75
119	W21	Type III	16	0.175	1.571	65.83	16.78	1.719	11.4	0.9	-0.213	10.75
120	W22	Type I	8	0.175	1.047	38.75	8.54	2.787	13.764	0.599	-0.161	10.75
121	W22	Type I	12	0.175	1.047	38.75	8.54	2.787	14.79	0.77	-0.332	10.75
122	W22	Type I	16	0.175	1.047	38.75	8.54	2.787	15.63	0.91	-0.472	10.75
123	W22	Type III	12	0.175	1.047	65.83	16.78	1.663	10.68	0.78	-0.093	10.75
124	W22	Type III	16	0.175	1.047	65.83	16.78	1.663	11.4	0.9	-0.213	10.75
125	W16	Type I	8	0.175	1.571	38.75	15.03	5.135	13.764	0.599	-0.469	19.4
126	W16	Type I	12	0.175	1.571	38.75	15.03	5.135	14.79	0.77	-0.640	19.4
127	W16	Type I	16	0.175	1.571	38.75	15.03	5.135	15.63	0.91	-0.780	19.4
128	W16	Type III	8	0.175	1.571	65.83	19.23	3.106	9.594	0.599	-0.181	19.4
129	W16	Type III	12	0.175	1.571	65.83	19.23	3.106	10.68	0.78	-0.362	19.4
130	W16	Type III	16	0.175	1.571	65.83	19.23	3.106	11.4	0.9	-0.482	19.4

Table 6A. Configuration dimensionless parameters

Test no	*Test ID*	*Bend*	L_{ARC}/T_W	R_C/T_W	L_{WPROJ}/T_W	D_{RATIO}	*A**	*2è/ð*
-	-	-	-	-	-	-	-	-
1	W03	Type I	1.02	2.815	0.300	0.778	27	1.00
2	W03	Type I	0.95	2.620	0.279	1.000	27	1.00
3	W03	Type I	0.90	2.479	0.264	1.182	27	1.00
4	W03	Type III	1.75	6.862	0.317	0.768	27	1.00
5	W03	Type III	1.57	6.164	0.285	1.000	27	1.00
6	W03	Type III	1.47	5.775	0.267	1.154	27	1.00
7	W02	Type I	1.53	2.815	0.300	0.778	27	1.00
8	W02	Type I	1.43	2.620	0.279	1.000	27	1.00
9	W02	Type I	1.35	2.479	0.264	1.182	27	1.00
10	W02	Type III	3.09	6.862	0.317	0.768	27	1.00
11	W02	Type III	2.77	6.164	0.285	1.000	27	1.00
12	W02	Type III	2.60	5.775	0.267	1.154	27	1.00
13	W01	Type I	1.23	2.815	0.300	0.778	27	1.00
14	W01	Type I	1.14	2.620	0.279	1.000	27	1.00
15	W01	Type I	1.08	2.479	0.264	1.182	27	1.00
16	W01	Type III	2.18	6.862	0.317	0.768	27	1.00
17	W01	Type III	1.96	6.164	0.285	1.000	27	1.00
18	W01	Type III	1.83	5.775	0.267	1.154	27	1.00
19	W04	Type I	0.62	2.815	0.161	0.778	10.75	1.00
20	W04	Type I	0.58	2.620	0.150	1.000	10.75	1.00
21	W04	Type I	0.55	2.479	0.142	1.182	10.75	1.00
22	W04	Type III	1.35	6.862	0.167	0.768	10.75	1.00
23	W04	Type III	1.22	6.164	0.150	1.000	10.75	1.00
24	W04	Type III	1.14	5.775	0.140	1.154	10.75	1.00
25	W05	Type I	0.75	2.815	0.161	0.778	10.75	1.00
26	W05	Type I	0.70	2.620	0.150	1.000	10.75	1.00
27	W05	Type I	0.66	2.479	0.142	1.182	10.75	1.00
28	W05	Type III	1.75	6.862	0.167	0.768	10.75	1.00
29	W05	Type III	1.57	6.164	0.150	1.000	10.75	1.00
30	W05	Type III	1.47	5.775	0.140	1.154	10.75	1.00
31	W06	Type I	0.83	2.815	0.236	0.778	19.4	1.00
32	W06	Type I	0.78	2.620	0.220	1.000	19.4	1.00
33	W06	Type I	0.74	2.479	0.208	1.182	19.4	1.00
34	W06	Type III	1.78	6.862	0.245	0.768	19.4	1.00
35	W06	Type III	1.60	6.164	0.220	1.000	19.4	1.00
36	W06	Type III	1.50	5.775	0.206	1.154	19.4	1.00
37	W07	Type I	1.01	2.815	0.236	0.778	19.4	1.00
38	W07	Type I	0.94	2.620	0.220	1.000	19.4	1.00
39	W07	Type I	0.89	2.479	0.208	1.182	19.4	1.00
40	W07	Type III	2.30	6.862	0.245	0.768	19.4	1.00
41	W07	Type III	2.07	6.164	0.220	1.000	19.4	1.00
42	W07	Type III	1.94	5.775	0.206	1.154	19.4	1.00

Test no	*Test ID*	*Bend*	L_{ARC}/T_W	R_C/T_W	L_{WPROJ}/T_W	D_{RATIO}	*A**	*2è/ð*
-	-	-	-	-	-	-	-	-
43	W08	Type I	0.62	2.815	0.167	0.778	10.75	0.67
44	W08	Type I	0.58	2.620	0.155	1.000	10.75	0.67
45	W08	Type I	0.55	2.479	0.147	1.182	10.75	0.67
46	W08	Type III	1.35	6.862	0.174	0.768	10.75	0.67
47	W08	Type III	1.22	6.164	0.156	1.000	10.75	0.67
48	W08	Type III	1.14	5.775	0.146	1.154	10.75	0.67
49	W09	Type I	0.75	2.815	0.167	0.778	10.75	0.67
50	W09	Type I	0.70	2.620	0.155	1.000	10.75	0.67
51	W09	Type I	0.66	2.479	0.147	1.182	10.75	0.67
52	W09	Type III	1.75	6.862	0.174	0.768	10.75	0.67
53	W09	Type III	1.57	6.164	0.156	1.000	10.75	0.67
54	W09	Type III	1.47	5.775	0.146	1.154	10.75	0.67
55	W10	Type I	0.81	2.815	0.234	0.778	19.4	0.67
56	W10	Type I	0.76	2.620	0.218	1.000	19.4	0.67
57	W10	Type I	0.72	2.479	0.206	1.182	19.4	0.67
58	W10	Type III	1.72	6.862	0.247	0.768	19.4	0.67
59	W10	Type III	1.54	6.164	0.221	1.000	19.4	0.67
60	W10	Type III	1.45	5.775	0.207	1.154	19.4	0.67
61	W11	Type I	0.98	2.815	0.234	0.778	19.4	0.67
62	W11	Type I	0.91	2.620	0.218	1.000	19.4	0.67
63	W11	Type I	0.86	2.479	0.206	1.182	19.4	0.67
64	W11	Type III	2.22	6.862	0.247	0.768	19.4	0.67
65	W11	Type III	1.99	6.164	0.221	1.000	19.4	0.67
66	W11	Type III	1.87	5.775	0.207	1.154	19.4	0.67
67	W12	Type I	1.00	2.815	0.293	0.778	27	0.67
68	W12	Type I	0.93	2.620	0.273	1.000	27	0.67
69	W12	Type I	0.88	2.479	0.258	1.182	27	0.67
70	W12	Type III	2.11	6.862	0.312	0.768	27	0.67
71	W12	Type III	1.90	6.164	0.280	1.000	27	0.67
72	W12	Type III	1.78	5.775	0.262	1.154	27	0.67
73	W13	Type I	1.20	2.815	0.293	0.778	27	0.67
74	W13	Type I	1.12	2.620	0.273	1.000	27	0.67
75	W13	Type I	1.06	2.479	0.258	1.182	27	0.67
76	W13	Type III	2.73	6.862	0.312	0.768	27	0.67
77	W13	Type III	2.45	6.164	0.280	1.000	27	0.67
78	W13	Type III	2.30	5.775	0.262	1.154	27	0.67
79	W14	Type I	1.01	2.815	0.300	0.778	27	0.83
80	W14	Type I	0.94	2.620	0.279	1.000	27	0.83
81	W14	Type I	0.89	2.479	0.264	1.182	27	0.83
82	W14	Type III	2.13	6.862	0.312	0.768	27	0.83
83	W14	Type III	1.91	6.164	0.280	1.000	27	0.83
84	W14	Type III	1.79	5.775	0.263	1.154	27	0.83
85	W15	Type I	1.22	2.815	0.300	0.778	27	0.83
86	W15	Type I	1.14	2.620	0.279	1.000	27	0.83
87	W15	Type I	1.08	2.479	0.264	1.182	27	0.83
88	W15	Type III	2.75	6.862	0.312	0.768	27	0.83
89	W15	Type III	2.47	6.164	0.280	1.000	27	0.83

Test no	*Test ID*	*Bend*	L_{ARC}/T_W	R_C/T_W	L_{WPROJ}/T_W	D_{RATIO}	*A**	*2è/ð*
-	-	-	-	-	-	-	-	-
90	W15	Type III	2.31	5.775	0.263	1.154	27	0.83
91	W17	Type I	0.83	2.815	0.373	4.597	19.4	1.00
92	W17	Type I	0.78	2.620	0.347	5.909	19.4	1.00
93	W17	Type I	0.74	2.479	0.329	6.984	19.4	1.00
94	W17	Type III	1.78	6.862	0.324	1.433	19.4	1.00
95	W17	Type III	1.60	6.164	0.291	1.866	19.4	1.00
96	W17	Type III	1.50	5.775	0.272	2.153	19.4	1.00
97	W18	Type I	0.83	2.815	0.357	4.597	19.4	0.67
98	W18	Type I	0.78	2.620	0.332	5.909	19.4	0.67
99	W18	Type I	0.74	2.479	0.314	6.984	19.4	0.67
100	W18	Type III	1.78	6.862	0.313	1.433	19.4	0.67
101	W18	Type III	1.60	6.164	0.281	1.866	19.4	0.67
102	W18	Type III	1.50	5.775	0.263	2.153	19.4	0.67
103	W19	Type I	1.01	2.815	0.373	4.597	19.4	1.00
104	W19	Type I	0.94	2.620	0.347	5.909	19.4	1.00
105	W19	Type I	0.89	2.479	0.329	6.984	19.4	1.00
106	W19	Type III	2.30	6.862	0.324	1.433	19.4	1.00
107	W19	Type III	2.07	6.164	0.291	1.866	19.4	1.00
108	W19	Type III	1.94	5.775	0.272	2.153	19.4	1.00
109	W20	Type I	0.98	2.815	0.357	4.597	19.4	0.67
110	W20	Type I	0.91	2.620	0.332	5.909	19.4	0.67
111	W20	Type I	0.86	2.479	0.314	6.984	19.4	0.67
112	W20	Type III	2.22	6.862	0.313	1.433	19.4	0.67
113	W20	Type III	1.99	6.164	0.281	1.866	19.4	0.67
114	W20	Type III	1.87	5.775	0.263	2.153	19.4	0.67
115	W21	Type I	0.62	2.815	0.209	1.368	10.75	1.00
116	W21	Type I	0.58	2.620	0.195	1.758	10.75	1.00
117	W21	Type I	0.55	2.479	0.184	2.078	10.75	1.00
118	W21	Type III	1.57	6.164	0.161	1.135	10.75	1.00
119	W21	Type III	1.47	5.775	0.151	1.310	10.75	1.00
120	W22	Type I	0.62	2.815	0.202	1.368	10.75	0.67
121	W22	Type I	0.58	2.620	0.188	1.758	10.75	0.67
122	W22	Type I	0.55	2.479	0.178	2.078	10.75	0.67
123	W22	Type III	1.57	6.164	0.156	1.135	10.75	0.67
124	W22	Type III	1.47	5.775	0.146	1.310	10.75	0.67
125	W16	Type I	1.09	2.815	0.373	4.597	19.4	1.00
126	W16	Type I	1.02	2.620	0.347	5.909	19.4	1.00
127	W16	Type I	0.96	2.479	0.329	6.984	19.4	1.00
128	W16	Type III	2.00	6.862	0.324	1.433	19.4	1.00
129	W16	Type III	1.80	6.164	0.291	1.866	19.4	1.00
130	W16	Type III	1.69	5.775	0.272	2.153	19.4	1.00

Table 7A. Configuration *MVR* and *AVR*

Test no	*Test ID*	*Bend*	MVR_O	MVR_I	MVR_C	AVR_O	AVR_I	AVR_C
-	-	-	-	-	-	-	-	-
1	W03	Type I	0.398	1.492	1.359	0.186	1.202	1.306
2	W03	Type I	0.354	1.370	1.358	0.120	1.232	1.255
3	W03	Type I	0.400	1.530	1.305	0.152	1.300	1.248
4	W03	Type III	0.266	1.580	1.714	0.113	1.398	1.462
5	W03	Type III	0.229	1.619	1.682	0.113	1.474	1.462
6	W03	Type III	0.194	1.569	1.699	0.182	1.503	1.409
7	W02	Type I	0.357	1.518	1.432	0.117	1.195	1.335
8	W02	Type I	0.285	1.578	1.327	0.113	1.294	1.276
9	W02	Type I	0.175	1.525	1.297	0.137	1.324	1.249
10	W02	Type III	0.267	1.371	1.653	0.171	1.244	1.292
11	W02	Type III	0.281	1.546	1.601	0.173	1.409	1.400
12	W02	Type III	0.401	1.562	1.750	0.294	1.495	1.398
13	W01	Type I	0.438	1.509	1.430	0.128	1.283	1.287
14	W01	Type I	0.210	1.537	1.302	0.101	1.347	1.284
15	W01	Type I	0.263	1.493	1.298	0.149	1.357	1.226
16	W01	Type III	0.203	1.523	1.680	0.138	1.378	1.440
17	W01	Type III	0.194	1.627	1.662	0.123	1.531	1.510
18	W01	Type III	0.250	1.694	1.708	0.129	1.573	1.485
19	W04	Type I	0.183	1.383	1.129	0.100	1.146	1.101
20	W04	Type I	0.357	1.382	1.243	0.187	1.216	1.160
21	W04	Type I	0.496	1.332	1.244	0.339	1.238	1.158
22	W04	Type III	0.765	1.147	1.288	0.649	1.066	1.099
23	W04	Type III	0.906	1.348	1.396	0.705	1.225	1.244
24	W04	Type III	0.978	1.387	1.380	0.839	1.269	1.265
25	W05	Type I	0.382	1.340	1.151	0.150	1.136	1.106
26	W05	Type I	0.438	1.345	1.182	0.239	1.183	1.121
27	W05	Type I	0.530	1.396	1.279	0.331	1.257	1.173
28	W05	Type III	0.871	1.198	1.190	0.741	1.012	1.111
29	W05	Type III	0.857	1.290	1.322	0.732	1.108	1.170
30	W05	Type III	1.197	1.419	1.519	0.900	1.245	1.367
31	W06	Type I	0.318	1.445	1.239	0.126	1.190	1.189
32	W06	Type I	0.230	1.496	1.308	0.082	1.301	1.248
33	W06	Type I	0.272	1.500	1.307	0.132	1.358	1.253
34	W06	Type III	0.390	1.324	1.477	0.209	1.134	1.223
35	W06	Type III	0.514	1.449	1.524	0.234	1.300	1.351
36	W06	Type III	0.546	1.507	1.456	0.357	1.339	1.332
37	W07	Type I	0.317	1.477	1.342	0.150	1.219	1.245
38	W07	Type I	0.262	1.514	1.269	0.117	1.267	1.230
39	W07	Type I	0.295	1.518	1.284	0.174	1.312	1.231
40	W07	Type III	0.614	1.203	1.562	0.350	1.148	1.306
41	W07	Type III	0.699	1.316	1.478	0.483	1.229	1.277
42	W07	Type III	0.642	1.462	1.561	0.395	1.362	1.372

43	W08	Type I	0.174	1.229	1.095	0.091	1.043	1.020
44	W08	Type I	0.216	1.321	1.132	0.131	1.138	1.040
45	W08	Type I	0.511	1.252	1.070	0.304	1.145	1.036
46	W08	Type III	0.612	1.252	1.336	0.419	1.090	1.157
47	W08	Type III	0.639	1.090	1.183	0.474	0.983	1.029
48	W08	Type III	0.774	1.214	1.289	0.551	1.130	1.144
49	W09	Type I	0.138	1.234	1.067	0.090	1.005	1.017
50	W09	Type I	0.275	1.256	1.083	0.156	1.097	1.025
51	W09	Type I	0.442	1.234	1.079	0.230	1.119	1.021
52	W09	Type III	0.669	1.102	1.226	0.448	0.989	1.074
53	W09	Type III	0.753	1.140	1.306	0.511	1.072	1.131
54	W09	Type III	0.761	1.287	1.338	0.565	1.169	1.178
55	W10	Type I	0.288	1.287	1.184	0.104	1.145	1.135
56	W10	Type I	0.126	1.216	1.176	0.076	1.119	1.065
57	W10	Type I	0.252	1.338	1.178	0.141	1.242	1.132
58	W10	Type III	0.269	1.398	1.443	0.185	1.166	1.251
59	W10	Type III	0.416	1.403	1.411	0.232	1.253	1.272
60	W10	Type III	0.518	1.467	1.430	0.285	1.346	1.311
61	W11	Type I	0.199	1.304	1.142	0.105	1.092	1.107
62	W11	Type I	0.255	1.300	1.203	0.164	1.176	1.131
63	W11	Type I	0.307	1.306	1.196	0.195	1.202	1.122
64	W11	Type III	0.401	1.317	1.398	0.243	1.170	1.252
65	W11	Type III	0.503	1.429	1.452	0.307	1.257	1.366
66	W11	Type III	0.635	1.378	1.529	0.385	1.330	1.330
67	W12	Type I	0.277	1.313	1.241	0.136	1.152	1.163
68	W12	Type I	0.185	1.288	1.187	0.103	1.195	1.125
69	W12	Type I	0.325	1.332	1.176	0.177	1.180	1.135
70	W12	Type III	0.164	1.346	1.700	0.094	1.279	1.452
71	W12	Type III	0.153	1.537	1.629	0.115	1.397	1.434
72	W12	Type III	0.374	1.605	1.580	0.190	1.454	1.424
73	W13	Type I	0.280	1.333	1.205	0.172	1.117	1.133
74	W13	Type I	0.313	1.289	1.146	0.124	1.173	1.105
75	W13	Type I	0.365	1.295	1.290	0.196	1.186	1.156
76	W13	Type III	0.135	1.212	1.469	0.105	1.153	1.127
77	W13	Type III	0.273	1.387	1.452	0.126	1.314	1.231
78	W13	Type III	0.287	1.506	1.654	0.229	1.448	1.307
79	W14	Type I	0.286	1.445	1.309	0.172	1.226	1.243
80	W14	Type I	0.263	1.409	1.326	0.096	1.312	1.252
81	W14	Type I	0.490	1.464	1.350	0.158	1.320	1.252
82	W14	Type III	0.180	1.476	1.691	0.113	1.314	1.409
83	W14	Type III	0.258	1.615	1.605	0.111	1.474	1.413
84	W14	Type III	0.262	1.560	1.631	0.182	1.490	1.400
85	W15	Type I	0.368	1.588	1.403	0.188	1.317	1.324
86	W15	Type I	0.390	1.421	1.309	0.115	1.283	1.235
87	W15	Type I	0.379	1.391	1.378	0.144	1.307	1.242
88	W15	Type III	0.290	1.313	1.640	0.161	1.180	1.296
89	W15	Type III	0.271	1.509	1.478	0.155	1.393	1.295
90	W15	Type III	0.394	1.514	1.564	0.249	1.452	1.347
91	W17	Type I	0.190	1.407	1.236	0.917	1.182	1.204
92	W17	Type I	0.269	1.369	1.285	0.089	1.249	1.176

93	W17	Type I	0.423	1.339	1.245	0.291	1.292	1.207
94	W17	Type III	0.180	1.411	1.263	0.501	1.072	1.160
95	W17	Type III	0.416	1.423	1.449	0.738	1.345	1.412
96	W17	Type III	0.476	1.465	1.535	0.878	1.393	1.378
97	W18	Type I	0.254	1.329	1.296	0.095	1.196	1.251
98	W18	Type I	0.253	1.338	1.243	0.139	1.219	1.199
99	W18	Type I	0.345	1.470	1.323	0.256	1.342	1.227
100	W18	Type III	0.243	1.339	1.452	0.219	1.146	1.279
101	W18	Type III	0.430	1.426	1.443	0.254	1.340	1.368
102	W18	Type III	0.565	1.500	1.549	0.392	1.427	1.413
103	W19	Type I	0.160	1.413	1.281	0.120	1.218	1.211
104	W19	Type I	0.286	1.316	1.214	0.142	1.234	1.150
105	W19	Type I	0.486	1.386	1.228	0.272	1.281	1.164
106	W19	Type III	0.342	1.260	1.352	0.076	1.124	1.172
107	W19	Type III	0.549	1.395	1.429	0.215	1.282	1.328
108	W19	Type III	0.610	1.308	1.405	0.367	1.270	1.321
109	W20	Type I	0.156	1.359	1.313	0.118	1.167	1.236
110	W20	Type I	0.202	1.392	1.317	0.112	1.269	1.243
111	W20	Type I	0.440	1.388	1.339	0.154	1.299	1.259
112	W20	Type III	0.388	1.337	1.482	0.103	1.239	1.403
113	W20	Type III	0.505	1.366	1.419	0.289	1.300	1.365
114	W20	Type III	0.595	1.413	1.390	0.405	1.349	1.371
115	W21	Type I	0.199	1.323	1.247	0.132	1.186	1.208
116	W21	Type I	0.481	1.237	1.190	0.146	1.138	1.095
117	W21	Type I	0.699	1.282	1.253	0.327	1.215	1.165
118	W21	Type III	0.872	1.236	1.254	0.172	1.118	1.181
119	W21	Type III	1.030	1.345	1.373	0.305	1.237	1.291
120	W22	Type I	0.193	1.331	1.191	0.484	1.125	1.164
121	W22	Type I	0.442	1.234	1.181	0.091	1.134	1.101
122	W22	Type I	0.740	1.317	1.238	0.111	1.217	1.130
123	W22	Type III	0.838	1.205	1.260	0.177	1.114	1.179
124	W22	Type III	0.988	1.237	1.368	0.168	1.170	1.260
125	W16	Type I	0.188	1.374	1.305	0.344	1.170	1.253
126	W16	Type I	0.305	1.369	1.264	0.451	1.234	1.171
127	W16	Type I	0.387	1.360	1.273	0.106	1.269	1.189
128	W16	Type III	0.302	1.265	1.566	0.302	1.198	1.284
129	W16	Type III	0.486	1.367	1.383	0.486	1.245	1.268
130	W16	Type III	0.579	1.471	1.493	0.579	1.339	1.324